Catalysis Science & Technology

ROYAL SOCIETY OF CHEMISTRY

MINI REVIEW

View Article Online
View Journal | View Issue

Cite this: *Catal. Sci. Technol.*, 2023, **13**, 4270

Functionalization of methane using molecular metal complexes as catalysts

Hiroto Fujisaki and Takahiko Kojima *

Received 10th May 2023,
Accepted 25th May 2023

DOI: 10.1039/d3cy00647f

rsc.li/catalysis

Efficient and selective functionalization of methane is one of the most important tasks in chemistry in light of its utilization as a naturally abundant feedstock toward the development of a sustainable society. This article surveys recent progress in oxidative conversion and C–H activation of methane to obtain useful functionalized products using molecular metal complexes as catalysts. The reactions proceed through C–H bond cleavage by high-valent metal–oxo complexes and also through C–H bond activation at lower-valent metal centers to form a C–O or C–C bond as a result of oxygen-rebound, reductive elimination or insertion processes. We also mention the importance of hydrophobic environments around metal centers to capture the methane molecule to be ready for the oxidative conversion toward the improvement of efficiency and product selectivity of CH_4 oxidation.

1. Introduction

Methane (CH_4) is an abundant C1 feedstock as a major component of natural gas, which is approximately 90%, and has been mainly used as a fuel and also as a raw material for producing many useful compounds including methanol.[1] Methane oxidation to afford methanol is quite important for further production of useful molecules including formaldehyde, acetic acid, dimethyl ether and so on.[2] Due to the serious situation in Europe, the natural gas supply has been reduced and alternative energy supplies have been considered such as renewables.[3] The reduced supply of natural gas causes inflation of the price and enforces us to develop more efficient methods to convert CH_4 to useful chemicals.[3] On the other hand, CH_4 shows 25-times higher global warming potential than CO_2;[4] thus, its discharge into air is avoided by flaring CH_4, which is an inevitable waste of the resource. The main strategy of large-scale CH_4 utilization is highly energy-consuming steam reforming to form syngas as a mixture of carbon monoxide (CO) and dihydrogen (H_2) in the presence of water and alumina-supported nickel catalysts at 1100 K.[5] In order to achieve efficient and selective conversion of methane, tremendous efforts have been devoted to the development of heterogeneous catalysts, including zeolite-based metal catalysts; however, these heterogeneous catalysts have been operated under harsh conditions including high temperature and high pressure.[6]

The difficulty of oxidative conversion of CH_4 to other compounds mainly stems from the high bond dissociation energy (BDE) of C–H bonds of CH_4, which is 105 kcal mol^{-1}.[7] The other difficulty is due to the fact that the BDE of C–H bonds of methanol (CH_3OH), which is a $2e^-$-oxidized product of CH_4, is 96 kcal mol^{-1}, lower than that of CH_4.[7] Therefore, the selective oxidation of CH_4 to obtain CH_3OH is very difficult due to overoxidation of CH_3OH to HCHO as a $4e^-$-oxidized product, which is much easier to oxidize to HCOOH as a $6e^-$-oxidized product.

As molecular and homogeneous catalysts that can oxidize CH_4 efficiently and selectively to afford CH_3OH, the most excellent performance can be found in the catalysis by methane monooxygenases (MMOs), which include metal ions such as Cu and Fe at the active sites to activate O_2 for generating oxidative active species.[8,9] These enzymes are Cu-containing particulate MMOs (pMMOs)[8] and Fe-containing soluble MMOs (sMMOs).[9] As for the crystal structure of sMMOs, a hydrophobic tunnel which is called the "W308 tunnel" is observed and the tunnel has been recognized to control the selectivity and accessibility of substrates, CH_4 and O_2, to let them react at the diiron centre through the formation of a reactive intermediate called "compound Q", which is a bis(μ-oxo) diiron(IV) species.[10] Any naturally occurring heme enzyme has never been reported to oxidize CH_4.

A number of small metal complexes as functional models of MMOs have been prepared to perform catalytic functionalization of alkanes to shed some light on the structure–reactivity relationship and to gain mechanistic insights into the reactions including the detection of intermediates involved such as high-valent metal–oxo complexes.[11] Although catalytic oxidation of gaseous alkanes including CH_4 has yet to be successful by using molecular

Department of Chemistry, Faculty of Pure and Applied Sciences, University of Tsukuba, Tsukuba, Ibaraki 305-8571, Japan. E-mail: kojima@chem.tsukuba.ac.jp

catalysts so far, it should be important to develop molecular catalysts for selective CH_4 functionalization to attain fundamental knowledge to gain a deeper understanding about reaction mechanisms and requisites for the selectivity and efficiency of the catalysis.

In this article, we focus on homogeneous molecular catalysts for methane oxidation, and thus, oxidative methane conversion using heterogeneous catalysts is not covered. Some examples of molecular catalysts supported on solid surfaces are also mentioned. Molecular catalysis includes a biomimetic approach inspired by metalloenzymes mentioned above and an organometallic strategy such as C–H activation.

2. Methane functionalization through C–H activation

In 1950, Snyder and Grosse reported the functionalization of methane to generate methane sulfonic acid (CH_3SO_3H; MSA) and methyl bisulfate (CH_3OSO_3H; MBS).[12] The process involved the use of $HgSO_4$ as a catalyst and SO_3 at 673 K and 93 bar of methane. The total conversion of methane to MSA/MBS was 44% in a 1 : 2 ratio; however, mechanistic insights into the catalytic process were not provided.[12] In 1993, Periana and colleagues reported a Hg-catalysed high-yield system in H_2SO_4.[13] This system involved the formation of $Hg(OSO_3H)_2$ as a catalyst by the reaction between $HgSO_4$ and H_2SO_4. The catalytic system involving $Hg(OSO_3H)_2$ achieved a turnover frequency (TOF) of 10^{-3} s^{-1} and 50% conversion of methane with 85% selectivity for MBS (CO_2 as the major by-product) at 350 K.[13] In the catalysis, H_2SO_4 acts as a reaction solvent, a reagent for esterification of methane, and an oxidant (Scheme 1).[13]

The first example of Pt-catalysed methane functionalization has been reported by Shilov.[14] In this system, K_2PtCl_4 and K_2PtCl_6 catalyse the conversion of methane to methanol and chloromethane under 10 MPa of methane at 393 K in water. Under these conditions, a low TON of <20 has been obtained due to decomposition of the catalyst to form Pt black.[14] The proposed mechanism involves three steps: (1) formation of a Pt^{II}–CH_3 intermediate through C–H activation of methane by a Pt^{II} complex, (2) oxidation of the Pt^{II}–CH_3 species with $PtCl_6^{2-}$ to form a Pt^{IV}–CH_3 complex, and (3) reductive elimination of CH_3OH or CH_3Cl from the Pt^{IV}–CH_3 species.[14]

In 1998, Periana and colleagues introduced a more effective Pt catalyst, dichloro(η^2-{2,2′-bipyrimidyl}) platinum(II) ([(bpym)$PtCl_2$]), known as the Periana catalyst.[15] The Periana catalyst, based on the Shilov system mentioned above,[14] converts methane to MBS with 90% conversion in oleum (fuming sulfuric acid; SO_3/H_2SO_4) at 500 K and 34 bar of methane. Under the conditions, MBS has been produced with a TON of 500 and a TOF of 10^{-3} s^{-1} with 81% selectivity.[15] The catalytic mechanism of the Periana-Catalytica system is depicted in Scheme 2.[16] The Periana-Catalytica system was significantly better than the Shilov system using K_2PtCl_4 due to the good solubility of Pt complexes with organic ligands.[17] More recently, a simplified Pt catalyst, $(DMSO)_2PtCl_2$, has been reported by Lee and co-workers.[18] This catalyst in oleum shows a very high TON of close to 20 000 and the highest MBS yield of 85% for 3 h under 35 bar of CH_4 and at 453 K. The role of the DMSO ligand, instead of bpym, is to increase the catalyst's stability and prevent deactivation to form $PtCl_2$ or PtO_2.[18] The Hg and Pt catalysts have a high reactivity in methane oxidation to MSA or MSB with high selectivity; however, these catalysts require prohibitively high Hg- and Pt-inventory costs. A practical metal-free process for producing MSA with 99% selectivity and 80% conversion of methane using only methane and SO_3 as reactants in H_2SO_4 has been also reported;[19] however, we do not go into detail about a metal-free system here.

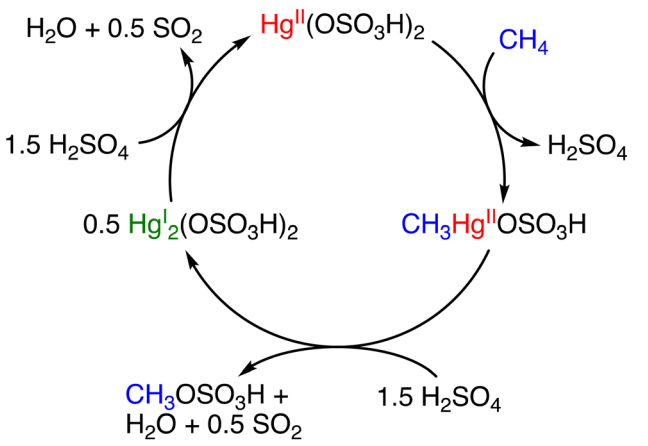

Scheme 1 Catalytic cycle for the methane activation with $Hg(OSO_3H)_2$ to generate MBS.[13]

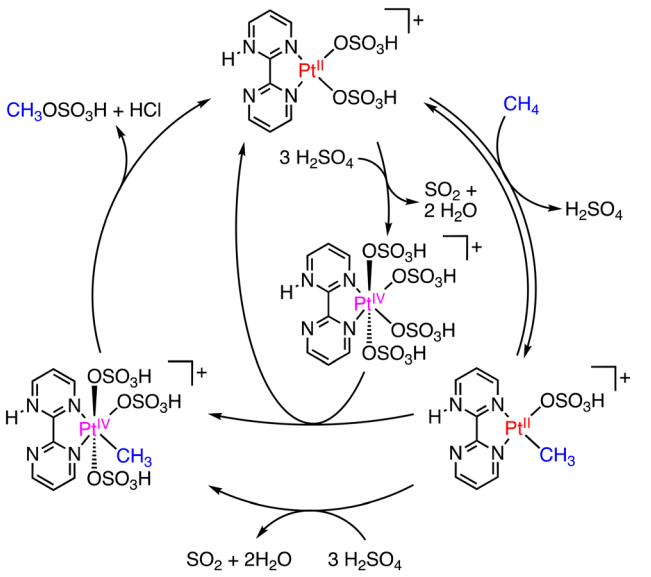

Scheme 2 Plausible mechanism in the Periana-Catalytica system to produce MBS.[16]

The aforementioned Hg- and Pt-catalysed methane-to-MSA or MBS conversion processes exhibit high methane conversion and MSA or MBS selectivity; however, adding water is required to hydrolyse MSA or MBS for methanol production. Therefore, the catalytic system needs to be further improved toward direct conversion of methane to methanol.

Other than the examples reported by Periana and co-workers,[15] C–H activation of CH_4 by Pd complexes having an *N*-heterocyclic carbene (NHC) ligand has been investigated.[20] Pd^{II}–NHC complexes catalysed the conversion of methane to CF_3COOCH_3 (MeTFA) with $K_2S_2O_8$ as an oxidant at 363 K and 30 bar of methane in CF_3COOH (HTFA) and $(CF_3CO)_2O$ (TFAA) (Fig. 1a). Under optimized conditions, a TON of 30 was obtained using $Pd^{II}Br_2$**L1** (**L1**: 1,1′-dimethyl-3,3′-methylenebisimidazolium dichloride) for 14 h as a catalyst (Fig. 1b).[20a] When an ethylene-bridged complex, $Pd^{II}Cl_2$**L2** (**L2**: 1,1′-dimethyl-3,3′-(1,2-dimethylene)bisimidazolium dichloride), was used as a catalyst (Fig. 1b), the TON was improved to 33 for 17 h.[20b] In 2009, Strassner and co-workers reported the pyrimidine–NHC Pd^{II} complex $[Pd^{II}Cl(\mathbf{L3})_2][Pd^{II}Cl_3(dmso)]$ (**L3**: 1-(2-pyrimidyl)-3-(methyl)imidazolium chloride) (Fig. 1b), which could functionalize methane to MeTFA with the highest TON of 41 for 17 h.[20c] These Pd–NHC complexes are suitable for C–H activation; the extraordinary thermal and chemical stability allows the reaction to proceed due to the suppression of the catalyst deactivation to form Pd black.[20]

On the other hand, Pd-catalysed oxidative functionalization of CH_4 has been achieved using O_2 as a terminal oxidant in HTFA in the presence of $NaNO_2$ as an NO source, although TONs are low (1–7) based on $[Pd^{II}]$.[21] In this reaction, CH_4 is assumed to undergo C–H activation at the Pd^{II} centre of $Pd^{II}(OAc)_2$ followed by ligand substitution to form a *cis*-$[CF_3COO–Pd^{II}–CH_3]$ intermediate, which affords MeTFA as the product through reductive elimination. The Pd^0 species formed *via* the reductive elimination is oxidized to a Pd^{II} species by quinone (Q). The quinone is reduced to hydroquinone (H_2Q), which is re-oxidized by NO_2 to regenerate Pd^{II} species. NO_2 is reduced to NO in the course of oxidation of H_2Q to Q and NO is oxidized by O_2 to recover NO_2 (Scheme 3).[21]

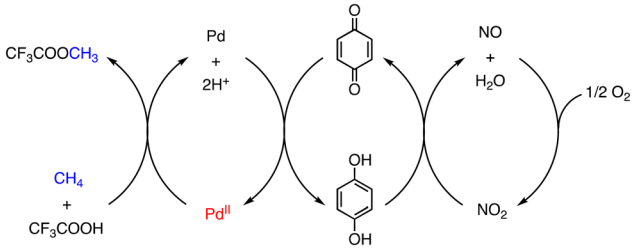

Scheme 3 Proposed reaction mechanism of a Pd^{II}/Q/NO_2/O_2 system to oxidize CH_4 in CF_3COOH.[21]

As another example of metal-salt-catalysed direct conversion of methane into MeTFA, Zeller and co-workers have reported a Co-catalysed oxidation system.[22] Yields of up to 50% based on methane were obtained using $Co(OAc)_2{\cdot}4H_2O$ as a pre-catalyst in HTFA/TFAA = 10 : 60 at 453 K under 20 bar of methane and 10 bar of O_2 as a terminal oxidant (Scheme 4). In this system, TFAA acts as an inhibitor of the deactivation of the catalyst by preventing the precipitation of the Co catalysts.[22]

In 2022, Lee and co-workers reported that $PdCl_4^{2-}$ can act as a catalyst to effectively convert methane to CF_3COOMe by using $K_2S_2O_8$ as an oxidant in HTFA in the presence of TFAA to remove water generated.[23] Under optimized conditions (catalyst: 0.01 mmol, $[K_2S_2O_8]$ = 10 mmol, [TFAA] = 24 mmol, HTFA: 30 g, under 20 bar of methane, 353 K, 15 h), $[Me_4N]_2[PdCl_4]$ shows the highest level of MeTFA production (TON 330, 33% selectivity) from methane oxidation.[23] The main overoxidized by-product is CO_2. The high catalytic reactivity of $[Me_4N]_2[PdCl_4]$ is derived from its ionic properties: a larger amount of $PdCl_4^{2-}$ can dissolve in the polar protic HTFA compared to the neutral Pd^{II} species, promoting the formation of a larger number of active catalytic species in the solution. During the catalytic reaction, $PdCl_4^{2-}$ is converted to $Pd(TFA)_4^{2-}$ as a pre-catalyst. Upon dissociation of one of the TFA ligands from $Pd(TFA)_4^{2-}$, the resulting complex reacts with methane to form *cis*-$[CF_3COO–Pd^{IV}–CH_3]$ as an intermediate, which then undergoes reductive elimination to afford MeTFA as the product (Scheme 5).[23]

The direct conversion of methane to MeTFA depicted in Scheme 5 exhibits high selectivity with the use of metal salts or metal complexes as catalysts and $S_2O_8^{2-}$ or O_2 as an oxidant in HTFA/TFAA. In addition, van Bokhoven and co-workers reported the same conversion with a TON of 33 for 17 h.[24] In this system, CuO has been employed as a pre-catalyst to form *in situ* an unknown homogeneous catalyst.[24]

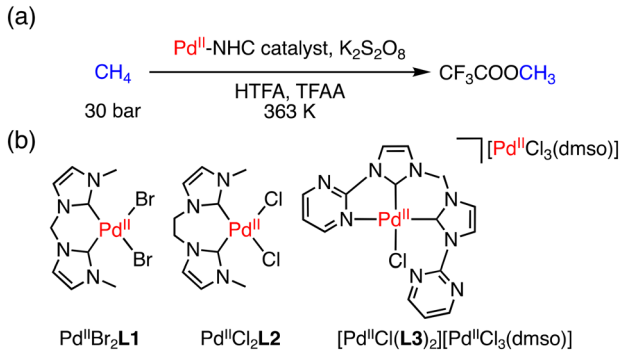

Fig. 1 (a) A schematic representation of conversion of methane to MeTFA; (b) structures of $Pd^{II}Br_2$**L1**, $Pd^{II}Br_2$**L1** and $[Pd^{II}Cl(\mathbf{L3})_2][Pd^{II}Cl_3(dmso)]$ as catalysts.[20]

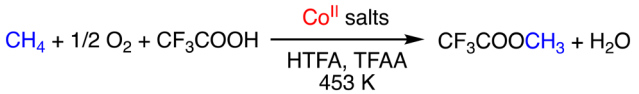

Scheme 4 Schematic representation of Co salt catalysed direct conversion of methane to MeTFA.[22]

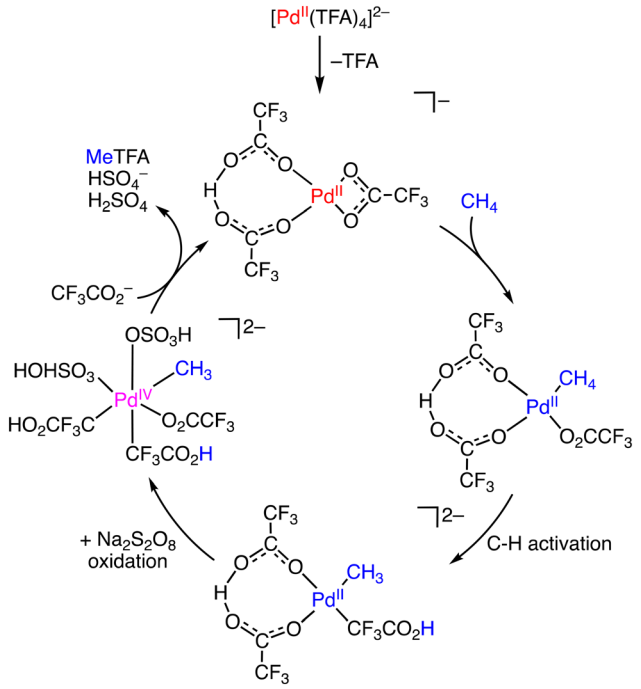

Scheme 5 Plausible reaction mechanism for methane oxidation using $Pd(TFA)_4^{2-}$.[23]

Other than the conversion of methane to MeTFA, C–H activation of CH_4 using transition metal complexes has been investigated using 4d- and 5d-transition metal complexes as catalysts. Two kinds of catalytic borylation of CH_4 have been achieved independently.[25] Sanford and co-workers have reported C–H borylation of CH_4 (2800 to 3500 kPa) using Ir, Rh, and Ru complexes as catalysts with bis-pinacolborane (B_2pin_2) in cyclohexane at 423 K as described in Scheme 6.[25] The products obtained are CH_3Bpin, $CH_2(Bpin)_2$, c-C_6H_{11}-Bpin, and HBpin. The product distribution can be controlled by the choice of catalysts. A dinuclear Ru(II) complex (Scheme 6), which acts as a pre-catalyst showing an induction period, afforded the ratio between CH_3Bpin and $CH_2(Bpin)_2$ of 21 : 1 and the highest selectivity between CH_3Bpin and c-$C_6H_{11}Bpin$ (83 : 1).[25] On the other hand, a Rh(I) complex (Scheme 6) exhibited the highest turnover number of 68 for 14 h with the ratio between CH_3Bpin and c-$C_6H_{11}Bpin$ of 46 : 1 and that between CH_3Bpin and $CH_2(Bpin)_2$ of 18 : 1 at the concentration of 0.75 mol% of the catalyst. The competitive reactions have been examined using mixtures of CH_4 (3500 kPa, 1.1 M) and CH_3Bpin (0.13 M, 1 equivalent to $(Bpin)_2$) as substrates, demonstrating that the reaction rate of CH_3Bpin formation is faster than that of the borylation of CH_3Bpin to afford $CH_2(Bpin)_2$ for the Ru catalyst; however, the Rh complex showed the opposite reactivity with a faster rate of borylation of CH_3Bpin than that of CH_4.[25] Note that the catalysts exhibited higher reactivity in CH_4 borylation than that of ethane.

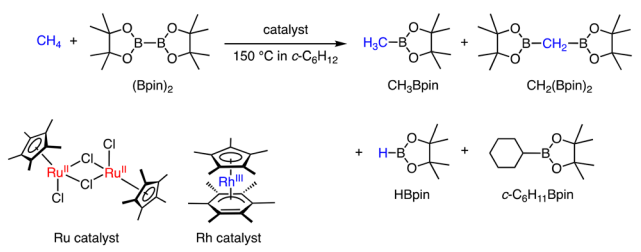

Scheme 6 Catalytic borylation of CH_4 by a Ru or Rh complex in c-C_6H_{12} at 423 K.[25]

At the same time, Mindiola and co-workers have reported catalytic borylation of CH_4 using Ir complexes bearing 1,10-phenathroline (phen) and its derivatives as ligands at 393 K in c-C_6H_{12} or THF.[26] They used dinuclear Ir^I complexes, $[Ir^I(COD)(\mu\text{-}X)]_2$ (COD = cyclooctadiene; X = Cl, OMe), as pre-catalysts. The phen ligands are added in a 2 : 1 molar ratio to the dimeric Ir^I complexes. In the case of the methoxo derivative, the products derived from CH_4 are CH_3Bpin, $CH_2(Bpin)_2$, and HBpin as in the case mentioned above.[25] Concomitantly, CH_3OBpin and ClBpin are also obtained as by-products derived from the bridging ligands, indicating that the dinuclear complexes turn to be mononuclear species during the reaction. The proposed reaction mechanism is depicted in Scheme 7.[26] The dimeric precursor complex is converted to a five-coordinated square-pyramidal Ir^I(phen) complex through the elimination of the bridging ligand and coordination of phen. The five-coordinate intermediate, which has been rationalized by DFT calculations, reacts with CH_4 to generate a *cis*-CH_3, H–Ir^{III}(phen) complex through

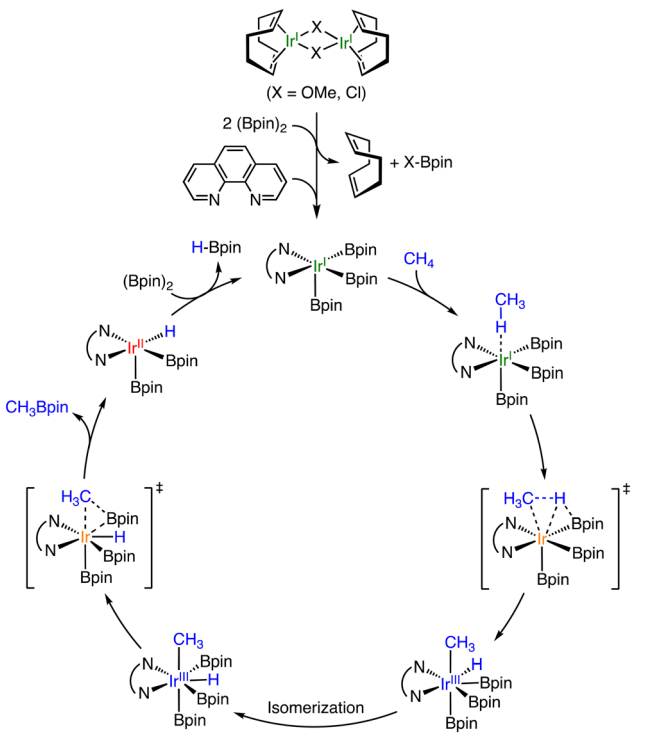

Scheme 7 A proposed mechanism of catalytic borylation of CH_4 by an Ir complex having phen as an auxiliary ligand.[26]

oxidative addition of CH_4. The intermediate is proposed to undergo isomerization, followed by reductive elimination of CH_3–Bpin as a product. Mindiola and co-workers have also reported catalytic borylation of CH_4 using [Ir^I(COD)(dmpe)] (dmpe = 1,2-bis(dimethylphosphino)-ethane) attached onto amorphous silica as a catalyst in c-C_6H_{12} or c-C_8H_{16} at 423 K.[27] The TON of borylation of CH_4 has been 12-fold improved by binding the molecular catalyst to the silica surface through the coordination of a Si–O^- moiety to the Ir centre. A proposed reaction mechanism is similar to that depicted in Scheme 7.[27]

Pérez and co-workers have reported that Ag complexes bearing perfluorinated tris(indazolyl)borate ligands catalyse the reaction of methane with ethyl diazoacetate (N_2-CHCOOEt) to yield ethyl propionate (CH_3CH_2COOEt).[28] F_{27}–$Tp^{4Bo,3CF2CF3}Ag$ (Fig. 2(a)) as a catalyst has afforded a TON of 478 in supercritical CO_2 (sc-CO_2) at 313 K and $P_{CH_4}:P_{CO_2}$ = 160 : 90 (Fig. 2a). In this reaction, sc-CO_2 was used as the solvent to dissolve the perfluorinated silver catalyst.[28] A plausible mechanism for C–H functionalization of methane to ethyl propionate involves Ag-catalysed N_2 elimination from ethyl diazoacetate followed by carbene transfer as depicted in Fig. 2(b).[28]

3. Formation of acetic acid using methane and CO

The oxidative coupling of methane with CO to form acetic acid has significant implications for the large-scale application of methane. Lin and Sen have reported a catalytic system that uses $RhCl_3$ as a catalyst and operates in an aqueous medium at 373 K (Scheme 8).[29] $RhCl_3$ acts as a catalyst in the production of acetic acid, methanol, and formic acid in the presence of methane (800 psi), CO (200 psi), and O_2 (100 psi). Additives such as HI and KI serve as promoters of the conversion to acetic acid by accelerating the formation of Rh–CH_3 species from methanol *via* methyl iodide formed *in situ*. Rh–CH_3 is then carbonylated to form a Rh–C(O)CH_3 species, which is subsequently hydrolyzed to form acetic acid. In the presence of KI (0.025 M), the yield of acetic acid has been improved more than two-fold from 34% to 80%.[29]

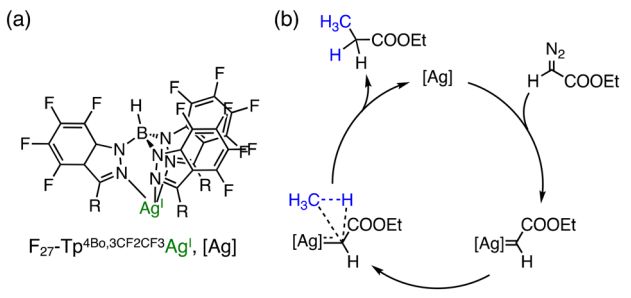

Fig. 2 (a) Schematic representation of F_{27}–$Tp^{4Bo,3CF2CF3}Ag$; (b) a plausible mechanism of Ag-catalysed methane functionalization in supercritical CO_2.[28]

$$CH_4 + CO + 1/2\ O_2 \xrightarrow[H_2O,\ 373\ K]{Rh^{III}Cl_3} CH_3COOH$$

Scheme 8 Schematic representation of methane to acetic acid conversion using $RhCl_3$.[29]

On the other hand, Periana and co-workers reported a Pd/H_2SO_4 system to afford acetic acid from methane.[30] The reaction is catalysed by Pd, and the results are consistent with a tandem catalysis mechanism, which involves methane C–H activation to generate Pd–CH_3 species affording methanol. Methanol is also converted to CO to react with the Pd–CH_3 intermediate to produce acetic acid. The origin of carbon sources of acetic acid has been confirmed by isotopic labelling experiments as shown in Scheme 9; with the use of a mixture of $^{12}CH_4$ and $^{13}CH_3OH$, $^{12}CH_3{}^{13}COOH$ was obtained as the product without forming $^{13}CH_3{}^{13}COOH$ or $^{13}CH_3{}^{12}COOH$.[30]

In 2007, Pombeiro and co-workers reported that vanadium complexes with N,O- or O,O-ligands can efficiently convert methane into acetic acid in HTFA under ambient conditions, using a peroxodisulfate salt, $K_2S_2O_8$, as an oxidant at 353 K.[31] The most effective catalysts were found to be triethanolaminate or (hydroxyimino)dicarboxylates, which lead to CH_3COOH production in 50% yield and high TONs up to 5.6×10^3.[31] Carboxylation proceeds through free radical mechanisms involving the sequential formation of $CH_3^{\bullet}$, CH_3-$CO^{\bullet}$, and $CH_3COO^{\bullet}$ upon H-abstraction. In this reaction, $S_2O_8^{2-}$ has been proposed to act as a source of sulfate radical anions ($SO_4^{\bullet-}$) and their protonated form ($HSO_4^{\bullet}$) that may act as H-abstractors from methane, as an oxidizing agent for vanadium, and as an oxidizing and coupling agent for CH_3-$CO^{\bullet}$. TFA is involved in the formation of CH_3COOH by carbonylating $CH_3^{\bullet}$, acting as an H-source to $CH_3COO^{\bullet}$, and enhancing the oxidizing power of a peroxo-V^V complex upon protonation.[31]

4. Photochemical oxidation of methane

In 2022, Groves and co-workers reported the photo-driven oxidation of methane to MeTFA using a commercial Fe^{III} source as a catalyst and dioxygen as the terminal oxygen in a mixture of HTFA and TFAA at a 4 : 1 ratio.[32] $Fe(OTf)_3$ was found to exhibit the best catalytic activity, producing a 60% yield of MeTFA with a TON of 24 based on the amount of Fe^{III} salt, without detectable overoxidation products. The reaction

$$^{13}CH_4 \xrightarrow[H_2SO_4,\ 453\ K]{Pd^{II}} {}^{13}CH_3{}^{13}COOH$$

$$^{12}CH_4 + {}^{13}CH_3OH \xrightarrow[H_2SO_4,\ 453\ K]{Pd^{II}} {}^{12}CH_3{}^{13}COOH + {}^{13}CH_3{}^{13}COOH + {}^{13}CH_3{}^{12}COOH$$

Scheme 9 Isotopic labelling for clarifying the origin of carbon sources of acetic acid.[30]

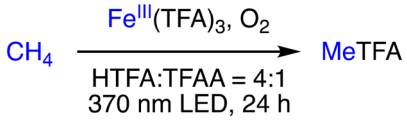

Scheme 10 Schematic representation of photocatalytic oxidation of methane to MeTFA.[32]

conditions involve a catalyst loading of 0.025 mmol, 15 mmol O_2, 100 psig of methane, 278 K, 370 nm LED, and 24 h reaction time. TFAA plays a crucial role in trapping H_2O as a by-product from O_2, similarly as mentioned above, to prevent deactivation of the $Fe^{III}(TFA)_3$ cluster (Scheme 10).[32] Note that the reaction mechanism of this system has yet to be clarified.

Photochemical functionalization of methane has been reported using Ce^{IV} salts as catalysts in CH_3CN under photoirradiation at 400 nm in the presence of 2,2,2-trichloroethanol (Cl_3CCH_2OH).[33] In the catalytic system, methylation of the C═C double bond of EtO(O)CC(H)═C(C(O)OEt)$_2$ was achieved to give the corresponding mono-methylated product in 58% yield (Scheme 11). Isoquinoline is methylated at the 1-position through Minisci-type nucleophilic alkylation in 19% yield. Di-*tert*-butyl azodicarboxylate (DBAD) is also methylated under the conditions to form an *N*-methyl hydralazine derivative through C–N bond formation. In those reactions, the initiation is LMCT in a Ce^{IV}–OCH_2CCl_3 complex to generate a Ce^{III} species and an alkoxo radical, $^{\bullet}OCH_2CCl_3$, which can abstract a hydrogen atom from CH_4 to form the methyl radical, $^{\bullet}CH_3$, as a nucleophilic reactant to C═C double bonds as well as aromatic rings.[33]

Another proposal has been raised by Schelter and co-workers on the Ce-catalysed methane oxidation reaction against the mechanism depicted in Scheme 11.[33,34] $[NEt_4]_2[CeCl_6]$ catalyses a coupling reaction of methane with diazo compounds to afford methylated hydrazine derivatives under photoirradiation at 390 nm at room temperature. The reaction is initiated by the formation of $Cl^{\bullet}$ as the oxidant through the photoinduced homolysis of a Ce^{IV}–Cl^- bond (Scheme 12). A yield of methane functionalization of 66%

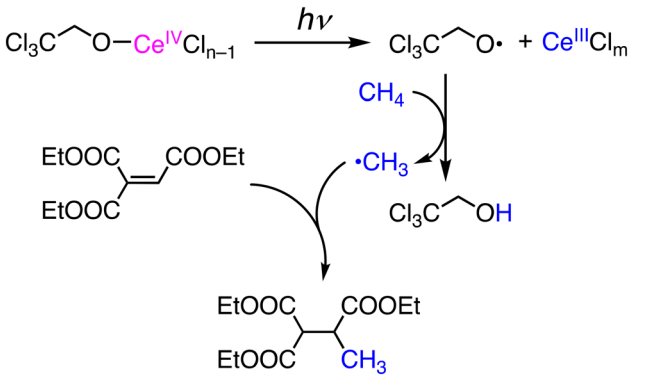

Scheme 11 Photoinduced functionalization of CH_4 based on LMCT in a Ce^{IV}–alkoxo complex to generate an alkoxy radical.[33]

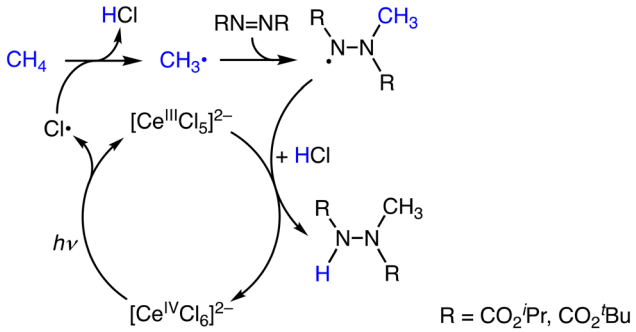

Scheme 12 Plausible reaction mechanism of the catalytic amination of methane using $[NEt_4]_2[CeCl_6]$.[34]

was obtained in the presence of $[NEt_4]Cl$ (25 mol%) and $HOCH_2CCl_3$ (20 mol%).[34] The presence of Cl^- in the reaction solution strongly affects the reactivity of the photocatalyst. This effect is due to the complexation of $Cl^{\bullet}$ with Cl^-, which can either stabilize or destabilize the radicals and affect the overall reaction pathway (Scheme 12).[34] The participation of $Cl^{\bullet}$ has been rationalized by the formation of chlorinated products in the presence of excess Cl^-.[34]

More recently, Noël and co-workers reported a new strategy to methane functionalization through hydrogen atom transfer using inexpensive decatungstate ($W_{10}O_{32}^{4-}$) as a photocatalyst at room temperature (Fig. 3).[35] $W_{10}O_{32}^{4-}$ undergoes hydrogen atom transfer from methane (45 bar) under photoirradiation at 365 nm to generate the methyl radical ($CH_3^{\bullet}$), which reacts with alkenes to afford hydroalkylated adducts in good yields and high selectivity in $CD_3CN:H_2O$ (7 : 1) at room temperature under flow conditions.[35] The reaction mechanism involves an excited state of $[W_{10}O_{32}]^{4-}$ ($^*[W_{10}O_{32}]^{4-}$) to abstract a hydrogen atom from a C(sp^3)–H bond of methane. After the formation of $CH_3^{\bullet}$, hydroalkylated adducts can be formed by trapping the radical with a variety of Michael acceptors (Fig. 3).[35]

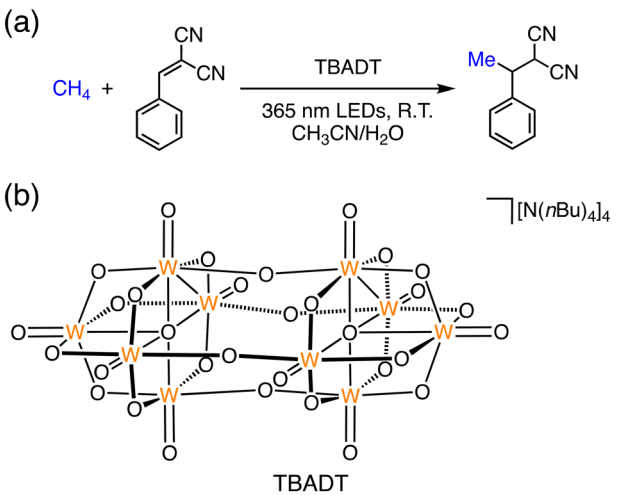

Fig. 3 (a) Schematic representation of the C(sp^3)–H functionalization of methane; (b) schematic description of the structure of $[N(nBu)_4]_4[W_{10}O_{32}]$ (TBADT).[35]

5. Catalytic oxidation of methane using peroxides

The first example of a molecular catalyst that can convert methane to methanol directly was reported in 1991 by Drago and co-workers with the use of H_2O_2.[36a] The sterically crowded *cis*-$[Ru^{II}(dmp)_2(S)_2]^{2+}$ (dmp = 2,9-dimethyl-1,10-phenanthroline) (S = MeCN or OH_2) complex is capable of methane hydroxylation under mild conditions using H_2O_2 as an oxidant (catalyst: 0.1 μmol, 30% aqueous H_2O_2: 0.1 mmol, under 4 atm of methane, 348 K, 30 h) (Scheme 13).[36a] Methanol and formaldehyde were obtained as main oxidation products with a total TON of 125 per day and 75% methanol selectivity. The reactive species of the catalytic cycle is assumed to be *cis*-$[Ru^{VI}(O)_2(dmp)_2]^{2+}$, which can be derived from a reaction of *cis*-$[Ru^{II}(dmp)_2(S)_2]^{2+}$ with H_2O_2 as a reactive species of the oxidation.[36b] Hydrogen atom transfer from CH_4 to the Ru=O moiety is followed by an oxygen-rebound process to form methanol bound to the Ru centre. Further ligand substitution of a bound methanol molecule with a solvent molecule (S) affords methanol and *cis*-$[Ru^{IV}(O)(dmp)_2(S)]^{2+}$.[36b] The *cis*-$[Ru^{VI}(O)_2(dmp)_2]^{2+}$ oxidant can then be regenerated from *cis*-$[Ru^{IV}(O)(dmp)_2(S)]^{2+}$ in the presence of excess H_2O_2.[36b]

A number of artificial catalysts have been developed to mimic the structures of pMMOs having multiple copper centres and sMMOs having a dinuclear iron site for catalysing methane oxidation under mild conditions.

As a functional model of pMMOs, in 2003, Chan and co-workers reported a tricopper cluster catalyst, $[Cu^ICu^ICu^I(7\text{-}N\text{-}Etppz)]^+$ (7-*N*-Etppz: 3,3′-(1,4-diazepane-1,4-diyl)bis[1-(4-ethyl piperazine-1-yl)propan-2-ol]) (Fig. 4a), which converts

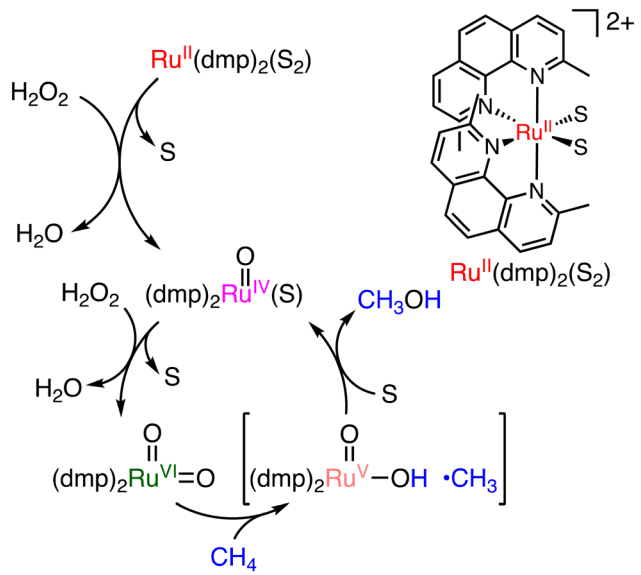

Scheme 13 A plausible mechanism of methane oxidation using $[Ru^{II}(dmp)_2(S)_2]^{2+}$ with H_2O_2 to form $[Ru^{VI}(dmp)_2(O)_2]^{2+}$ as a reactive species (S = MeCN or H_2O).[36b]

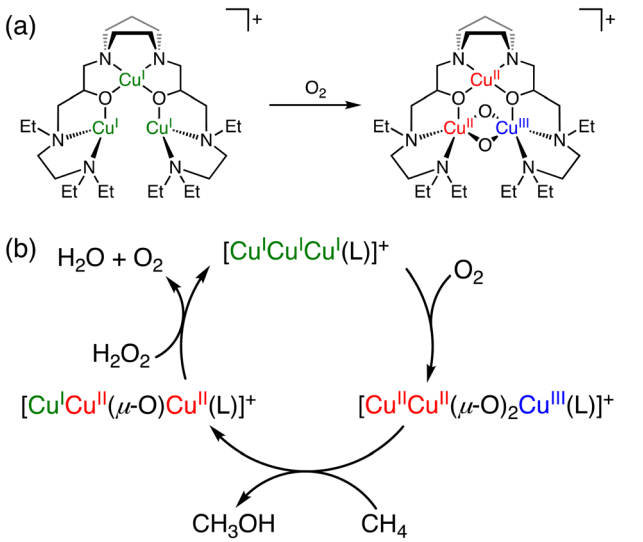

Fig. 4 (a) The schematic representation of reaction of $[Cu^ICu^ICu^I(7\text{-}N\text{-}Etppz)]^+$ with O_2 to form $[Cu^{II}Cu^{II}(\mu\text{-}O)_2Cu^{III}(7\text{-}N\text{-}Etppz)]^+$.[37,38] (b) A proposed mechanism of methane oxidation with $[Cu^ICu^ICu^I(7\text{-}N\text{-}Etppz)]^+$ with the use of O_2 and H_2O_2.[38]

methane to methanol in acetonitrile at room temperature using molecular oxygen and hydrogen peroxide.[37,38] Under optimized conditions ([catalyst] = 8 mM, $[H_2O_2]$ = 160 mM, $[CH_4]$ = 11 mM, under an O_2 atmosphere, 1 h), the tricopper cluster catalyst exhibits a TON of 7 with 100% methanol selectivity.[38] During the catalytic cycle, $[Cu^ICu^ICu^I(7\text{-}N\text{-}Etppz)]^+$ reacts with molecular oxygen to form $[Cu^{II}Cu^{II}(\mu\text{-}O)_2\text{-}Cu^{III}(7\text{-}N\text{-}Etppz)]^+$ as the active species, which is responsible for the methane oxidation to afford methanol. H_2O_2 has been proposed to be required as a reductant for regenerating $[Cu^I\text{-}Cu^ICu^I(7\text{-}N\text{-}Etppz)]^+$ from $[Cu^ICu^{II}(\mu\text{-}O)Cu^{II}(7\text{-}N\text{-}Etppz)]^+$, which is an intermediate formed concomitantly with methanol (Fig. 4b).[38,39] Furthermore, the TON of methane oxidation was improved to 18 under modified conditions, where 20 equivalents of H_2O_2 were used to initiate the reaction, followed by incremental dropwise additions of the same amount of H_2O_2 at 10 minute intervals.[40] One of the advantages of this reaction is high methanol selectivity in methane oxidation. The disadvantages, however, include a low TON, the use of an organic solvent, and catalyst deactivation caused by hydrogen peroxide.[41]

More recently, Kodera and co-workers have reported a dinuclear Cu complex, $[Cu_2(\mu\text{-}OH)(6\text{-}hpa)]^{3+}$ (hpa = 1,2-bis{2-[bis(2-pyridylmethyl)aminomethyl]pyridine-6-yl}ethane), which can oxidize methane to methanol and formaldehyde in MeCN/H_2O (4 : 1) at 323 K using H_2O_2 as an oxidant.[42] In this reaction, methyl hydroperoxide (CH_3OOH) is obtained as the major product and formaldehyde as a minor product. The TON_{MeOH}, TON_{HCHO} and TON_{total} were determined to be 43, 7.4 and 50.4 after the treatment of PPh_3 to convert MeOOH to MeOH (Fig. 5a). In this catalytic system, $[Cu_2(O^{\bullet})(O_2^{\bullet})(6\text{-}hpa)]^{2+}$ has been proposed to be formed as a reactive species through the reaction of $[Cu_2(\mu\text{-}OH)(6\text{-}hpa)]^{3+}$ with H_2O_2 (Fig. 5b). Based on the DFT calculations, the Cu^{II}–$O^{\bullet}$ moiety

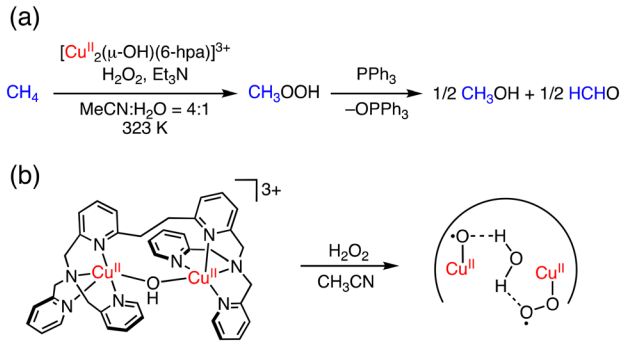

Fig. 5 (a) Methane oxidation with H_2O_2 catalysed by [Cu_2(μ-OH)(6-hpa)]$^{3+}$. (b) Plausible active species of benzene oxidation by [Cu_2(μ-OH)(6-hpa)]$^{3+}$ with H_2O_2.[42]

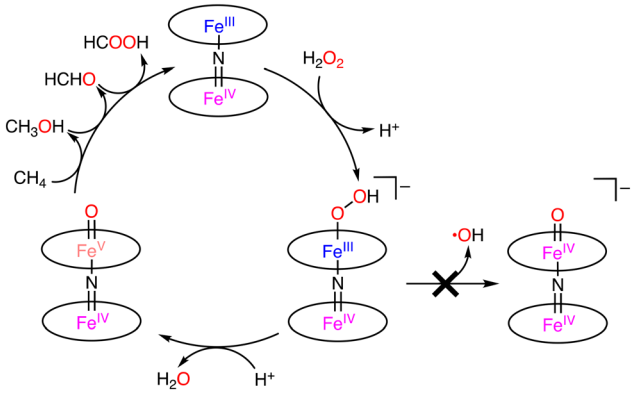

Scheme 15 Proposed mechanism of the formation of active species in the system.[44–46]

of the active species should have a high oxidation ability to cleave the strong C–H bond of methane.[42]

Nitride-bridged dinuclear iron phthalocyanine complexes, $(FePc)_2N$, are designed on the basis of the diiron active site of sMMOs.[9] $(FePc)_2N$ contains 2 equivalent Fe centres with a +3.5-oxidation state linearly bridged by the nitride ligand (Scheme 14).[43] In 2008, Bouchu and co-workers reported an iron μ-nitrido tetra-*tert*-butylphthalocyanine, $(FePc^tBu_4)_2N$ complex, which can oxidize methane with H_2O_2 as an oxidant in water.[44]

Under optimized conditions (catalyst: 0.925 μmol, H_2O_2: 678 μmol, under 32 bar of CH_4, 20 h), the maximum total TON of 84 was obtained at 323 K.[44] The selectivity to methanol, formaldehyde, and formic acid was 0%, 32%, and 68%, respectively.[44] The key step of the catalytic reaction is the formation of $Fe^{IV}NFe^{V}$=O by the reaction between $(FePc^tBu_4)_2N$ and H_2O_2. $Fe^{IV}NFe^{IV}$=O or $Fe^{IV}NFe^{V}$=O was formed by the O–O bond cleavage in $Fe^{IV}NFe^{III}OOH$. In the homolytic O–O bond cleavage, $Fe^{IV}NFe^{IV}$=O and the hydroxy radical (•OH) would be formed. In this case, $(FePc^tBu_4)_2N$ would be decomposed by the strongly oxidizing •OH. On the other hand, $Fe^{IV}NFe^{V}$=O and $^-$OH were formed through the heterolytic O–O bond cleavage. In this catalytic system, the Fe–N–Fe unit of $(FePc^tBu_4)_2N$ plays an important role in the catalytic reactivity by stabilizing the high-valent Fe–oxo intermediate with the strongly electron-donating μ-nitride ligand.[44–46] Therefore, the proposed mechanism involves the heterolytic μ-nitrido tetra-*tert*-butylphthalocyanine cleavage of the O–O bond, leading to the formation of a highly oxidizing $Fe^{IV}NFe^{V}$=O species, which is generated by the release of an H_2O molecule from the $Fe^{IV}NFe^{III}OOH$ complex in the presence of an acid (Scheme 15).[44–46]

In 2012, Sorokin and co-workers reported an oxo-diiron(IV) porphyrin π-radical complex, which was obtained from the reaction of a nitride-bridged diiron *meso*-tetraphenylporphyrin complex, $[(TPP)Fe^{III}(\mu\text{-}N)Fe^{IV}(TPP)]^0$, with *m*-chloroperbenzoic acid (*m*CPBA) as an oxygen atom transfer reagent (Scheme 16).[47] Catalytic methane oxidation was achieved using a silica-supported $[(TPP)Fe^{III}(\mu\text{-}N)Fe^{IV}(TPP)]^0$ catalyst, $[(TPP)Fe^{III}(\mu\text{-}N)Fe^{IV}(TPP)]^0$–$SiO_2$, and 100 equivalents of *m*CPBA. The overoxidized product, formic acid, was obtained in a yield of 44% based on the oxidant. The result indicates that $[(TPP)(\mu\text{-}CBA)Fe^{IV}(\mu\text{-}N)Fe^{IV}(O)(TPP^{\bullet+})]^-$, which is proposed as an active species of this catalytic system, should have a comparable oxidizing ability to that of putative $Fe^{IV}NFe^{V}$=O species derived from $(FePc^tBu_4)_2N$.[44–47]

More recently, Tanaka and co-workers reported the utilization of supramolecular catalysts based on a nitride-bridged iron porphyrinoid dimer using a porphyrin–phthalocyanine heterodimer connected *via* a four-fold rotaxane structure (Scheme 17).[48,49] The μ-nitride $[(Por)Fe\text{–}N\text{–}Fe(Pc)]^{5+}$ complex with a terminal stopper and tetraanionic metalloporphyrin (M-$TPPS^{4-}$, 5,10,15,20-tetrakis(4-sulfonatophenyl) porphyrin metal complex, M = Cu(II) or

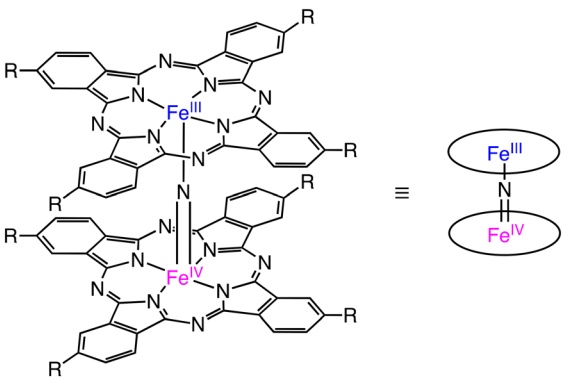

Scheme 14 The schematic representation of $(FePcR_4)_2N$.[43]

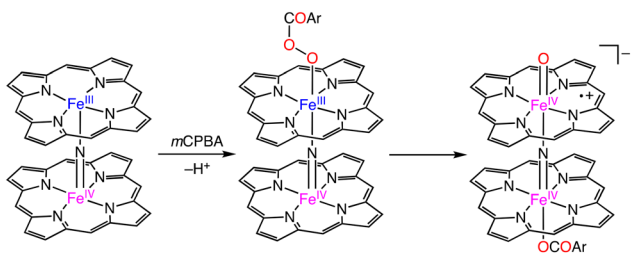

Scheme 16 Proposed mechanism for the formation of the N-bridged high-valent diiron–oxo porphyrin cation radical complex.[47]

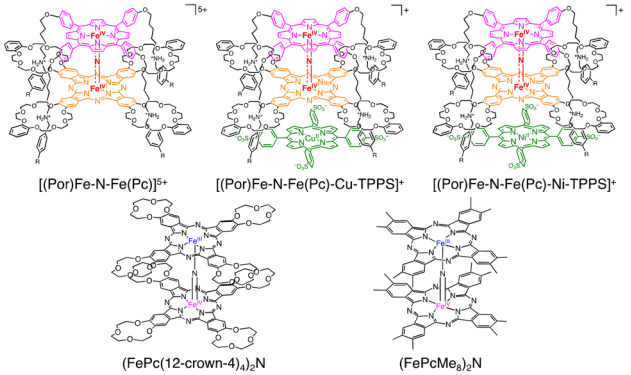

Scheme 17 Schematic representations of supramolecular extension of a μ-nitrido-bridged dinuclear iron complex of a four-fold rotaxane heterodimer of a porphyrin and a phthalocyanine.[49–51]

Ni(II)) resulted in the extension of the stacked structure to form $[(Por)Fe–N–Fe(Pc)–M–TPPS]^+$ through π–π stacking and electrostatic interaction, as depicted in Scheme 17. Under optimized conditions ([silica supported catalyst] = 141 μM, $[H_2O_2]$ = 160 mM, [HTFA] = 51 mM, under 1 MPa of methane, solvent: H_2O, 333 K, 8 h), the reactivity of the supramolecular catalysts in methane oxidation was enhanced *via* electron donation through π–π stacking to afford a maximum total TON of *ca.* 50.[50] Furthermore, Tanaka and co-workers reported $(FePc(12\text{-crown-}4)_4)_2N$ and $(FePcMe_8)_2N$ complexes bearing an electron-donating group on phthalocyanine moieties (Scheme 17).[50,51] The catalytic activity of $(FePc(12\text{-crown-}4)_4)_2N$ and H_2O_2 was lower than that of $(FePc^tBu_4)_2N$ due to the decomposition of 12-crown-4 moieties during the reaction.[50] In contrast, the total TON reached 100 using $(FePcMe_8)_2N$–SiO_2 as a silica-supported catalyst and H_2O_2 as an oxidant.[51] Sorokin and de Visser proposed that the introduction of electron-donating substituents is advantageous for H atom abstraction due to increasing the basicity of the oxo species.[52] Based on the lack of the catalytic oxidation reaction in the presence of excess Na_2SO_3 as a radical scavenger, Tanaka proposed the possibility of a Fenton-type reaction,[53–55] in which the ˙OH radical acts as a reactive species instead of $Fe^{IV}NFe^{V}$=O (Scheme 18).[49–51] In addition, the bleaching of the colour of catalysts and overoxidation of oxidized products were observed.[49–51]

Therefore, strategies to suppress the overoxidation of the oxidized products and the decomposition of the catalyst need to be developed for efficient and selective oxidation of methane.

6. Molecular catalysts having hydrophobic moieties in the second coordination sphere for methane oxidation

To mimic the catalytic oxidation of organic substrates by natural enzymes, heme model complexes have been intensively studied and the high reactivity has been reproduced by the model complexes so far.[56,57] In order to oxidize methane efficiently, a methane molecule should be trapped in the vicinity of an active metal centre, which can be converted to a reactive state as observed in enzymatic oxidation reactions.

As for the introduction of a hydrophobic second coordination sphere (SCS) which can bind to a methane molecule in the close vicinity of a metal centre, Martinez and co-workers have reported the capture of a methane molecule by a hemicryptophane (Hm) moiety attached to metal–pyridylamine complexes as a hydrophobic cavity; the ^1H NMR signal attributed to the methane molecule showed a significant upfield shift, indicating the interaction of the methane molecule with Hm.[58]

In methane oxidation reactions by using a silica-supported $[Cu^{II}(Hm–TREN)]^{2+}$ (TREN: tris(2-aminoethyl) amine) catalyst and naked $[Cu^{II}(TREN)]^{2+}$, total TONs of 2 and 1 have been obtained, respectively, indicating no significant changes in the reactivity (reaction conditions: silica supported catalyst: 1.0 μmol, $[H_2O_2]$ = 0.33 M, $[H_2SO_4]$ = 0.07 M, 30 bar of methane, 333 K, 20 h) (Scheme 19).[58] Martinez and co-workers have reported oxido-vanadium(V)

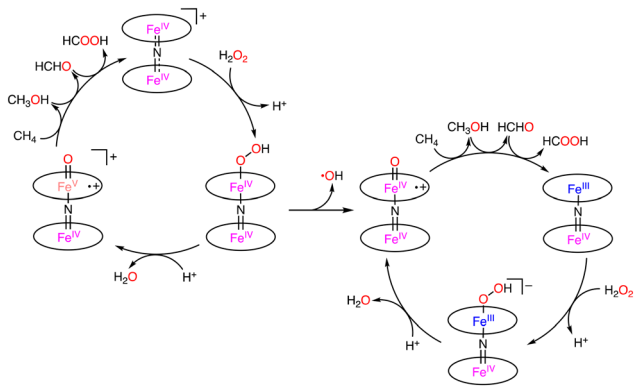

Scheme 18 Plausible reaction mechanism for methane oxidation by $[(Por)Fe–N–Fe(Pc)]^{5+}$.[49–51]

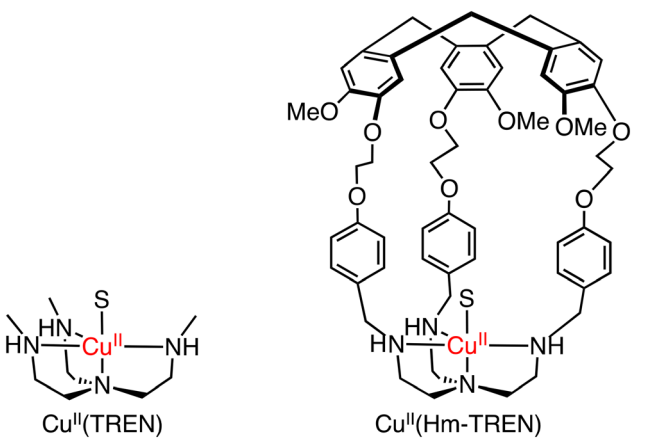

Scheme 19 The schematic representations of Cu(TREN) and Cu^{II}(Hm–TREN). S: solvent.[58]

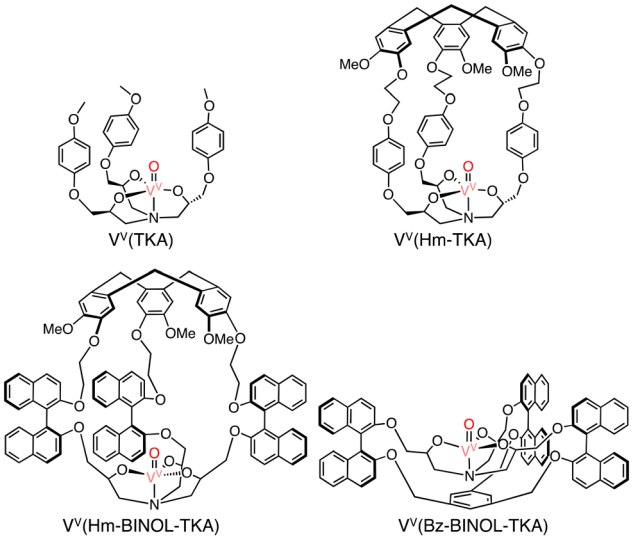

Scheme 20 The schematic representations of V^V(TKA), V^V(Hm–TKA), V^V(Hm–BINOL–TKA) and V^V(Bz–BINOL–TKA).[58]

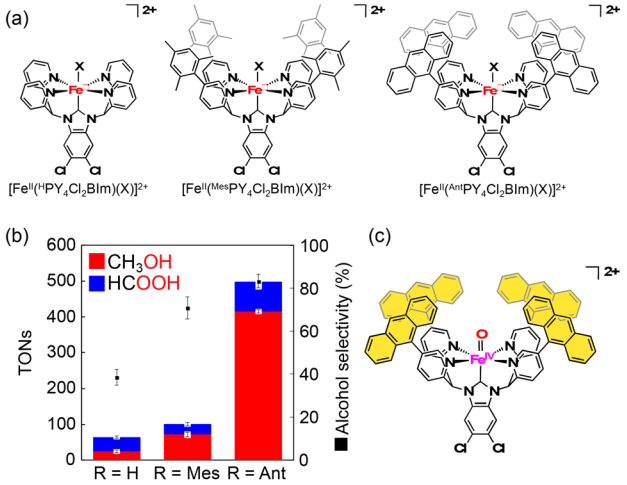

Fig. 6 (a) Schematic representations of $[Fe^{II}(^{R}PY_4Cl_2BIm)(X)]^{2+}$ (R = H, Mes, Ant, X: OH_2, OD_2, $NCCH_3$ or NCC_6H_5). (b) Comparison of TONs and alcohol selectivity among the three catalysts. (c) Schematic representation of active species for methane oxidation by $[Fe^{II}(^{Ant}PY_4Cl_2BIm)(OH_2)]^{2+}$ and $Na_2S_2O_8$ in H_2O : CH_3CN = 95 : 5.[62]

complexes that can act as catalysts for sulfoxidation of thioanisole with the use of alkyl hydroperoxides (^{t}BuOOH and cumyl-OOH) as oxidants in CH_2Cl_2.[59,60] The complexes have nitrilotriacetic-acid-based tripodal ligands and are referred to as V^V(Hm–TKA), V^V(Hm–BINOL–TKA), and V^V(Bz–BINOL–TKA) bearing the respective hydrophobic SCS near the metal centre (Scheme 20).[59,60]

The same complexes have been applied as catalysts to methane oxidation. The introduction of a hydrophobic SCS led to an increase in the yield of oxidized products in oxidation of methane (30 bar) using H_2O_2 as an oxidant in H_2O at 60 °C.[58] V^V(Bz–BINOL–TKA) was found to be the most effective catalyst with a TON of 18.3 (20 h), higher than those of V^V(TKA), V^V(Hm–TKA), and V^V(Hm–BINOL–TKA), although the highest selectivity to 2-electron-oxidized products (CH_3OH and CH_3OOH) has been observed for V^V(Hm–TKA) to be 15%.[58] These results suggest that the size and shape of the hydrophobic SCS have a significant impact on the efficiency of methane oxidation. Methane oxidation was also achieved by using silica-supported $[Fe^{II}$(Hm–TPA)$]^{2+}$ (TPA: tris(2-pyridyl-methyl)amine) having the Hm moiety at the TPA ligand as a catalyst (Scheme 21) and H_2O_2 as an oxidant. Introducing the Hm moiety to the Fe–TPA complex has improved the total TON from 4.7 to 9.7 and the selectivity to CH_3OH and CH_3OOH from 15% to 27%.[58]

Although these results demonstrate the positive impact of the hydrophobic SCS on the efficiency in terms of TONs and the selectivity to 2-electron-oxidized products such as CH_3OH and CH_3OOH, very low TONs have been observed. Therefore, one of the most promising approaches to suppressing the overoxidation is the use of catalysts with a

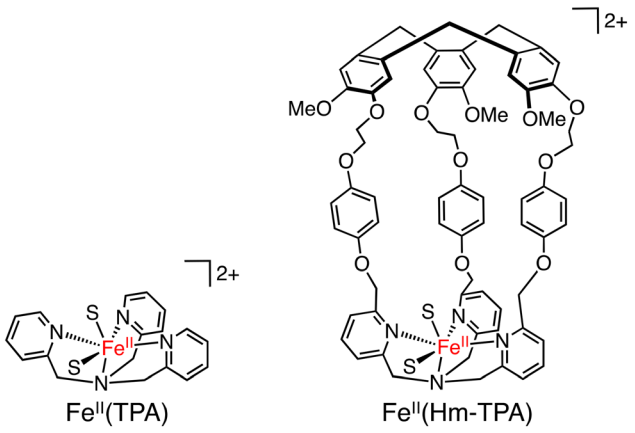

Scheme 21 The schematic representations of Fe^{II}(TPA) and Fe^{II}(Hm–TPA). S: solvent.[58]

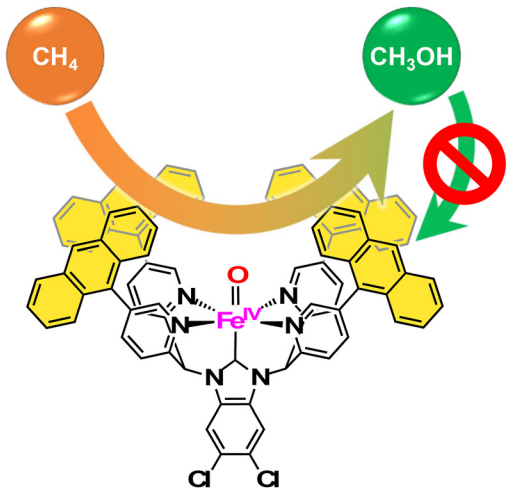

Fig. 7 The concept of "catch and release" strategy to suppress the overoxidation for selective conversion of methane to methanol.[62]

Table 1 Summary of catalytic C–H activation of methane

Catalysts and conditions	Solvent	Reaction time	Total TON	Product, selectivities	Ref.
$HgSO_4$[a]	H_2SO_4	—	—	MSA, 38%; MBS, 62%	12
$Hg(OSO_3H)_2$[b]	H_2SO_4	3 h	11	MBS, 85%	13
K_2PtCl_4, K_2PtCl_6	H_2O	0.25–5 h	<20	MeOH, —; $CHCl_3$, —	14
$[(bpym)PtCl_2]$[c]	H_2SO_4	3 h	500	MBS, 84%; CO_2, 16%	15 and 18
K_2PtCl_4[c]	H_2SO_4	3 h	17 000	MBS, 62%; CO_2, 38%	18
$(DMSO)_2PtCl_2$[c]	H_2SO_4	3 h	20 000	MBS, 85%; CO_2, 15%	18
$[Pd^{II}Cl(\mathbf{L3})_2][Pd^{II}Cl_3(dmso)]$[d]	HTFA, TFAA	17 h	41	MeTFA, 100%	20
$Pd(OAc)_2$, quinone, $NaNO_2$, O_2[e]	HTFA	10 h	7	MeTFA, 100%	21
$Co(OAc)_2{\cdot}4H_2O$, O_2[f]	HTFA, TFAA	24 h	13	MeTFA, 100%	22
$[Me_4N]_2[PdCl_4]$, $K_2S_2O_8$[g]	HTFA, TFAA	15 h	330	MeTFA, 45%; CO_2, 55%	23
CuO, $K_2S_2O_8$[h]	HTFA, TFAA	17 h	33	MeTFA, 86%	24
$(MesH)Ir(Bpin)_3$, B_2pin_2[i]	c-C_6H_{12}	14 h	15	CH_3Bpin, 63%; CyBpin, 21%; $CH_2(Bpin)_2$, 16%	25
Cp*Rh, B_2pin_2[i]	c-C_6H_{12}	14 h	33	CH_3Bpin, 89%; CyBpin, 1%; $CH_2(Bpin)_2$, 10%	25
Cp*RuCl(μ-Cl)$_2$RuClCp*, B_2pin_2[i]	c-C_6H_{12}	14 h	22	CH_3Bpin, 94%; CyBpin, 1%; $CH_2(Bpin)_2$, 5%	25
$[Ir(COD)(\mu\text{-}Cl)]_2$, dmpe, B_2pin_2[j]	c-C_6H_{12}	16 h	104	CH_3Bpin, 75%; $CH_2(Bpin)_2$, 25%	26
$[(dmpe)Ir(cod)CH_3]$–SiO_2, B_2pin_2[k]	c-C_8H_{16}	16 h	1857	CH_3Bpin, >99%	27
F_{27}–$Tp^{4Bo,3CF2CF3}Ag$, $N_2CHCOOEt$[l]	Sc–CO_2	14 h	478	CH_3CH_2COOEt, 100%	28
$RhCl_3$, CO, O_2, HCl, KI[m]	H_2O	352 h	3.8	CH_3COOH, 71%; CH_3OH, 2%; HCOOH, 27%	29
$PdSO_4$[n]	H_2SO_4	7 h	18	CH_3COOH, 72%; CH_3OH, 17%; CO_2, 11%	30
$VO\{N(CH_2CH_2O)_3\}$, $K_2S_2O_8$, CO[o]	TFA	20 h	5.6×10^3	CH_3COOH, 100%	31
$Fe(TFA)_3$, O_2, $h\nu$[p]	HTFA, TFAA	24 h	24	MeTFA, 56%; CO_2, 44%	32
$Ce(OTf)_3$, CCl_3CH_2OH, TBACl, DBAD, $h\nu$[q]	CH_3CN	18 h	2900	$CH_3N(Boc)NH(Boc)$, 100%	33 and 34
TBADT, alkenes[r]	$CD_3CN:H_2O = 7:1$	6 h	<200	Corresponding hydroalkylated adducts, <90%	35

[a] Reaction conditions: $SO_3:CH_4$ = 6.9, 93.1 bar of methane, 673 K. [b] Catalyst: 2.0 mmol, TFA: 2.0 mmol, 34.5 bar of methane, 453 K. [c] [Catalyst] = 0.77 mM, 35 bar of methane, 453 K. [d] $[Pd^{II}Cl(\mathbf{L3})_2][Pd^{II}Cl_3(dmso)]$: 0.084 mmol, $K_2S_2O_8$: 8.4 mmol, HTFA: 32 mL, TFAA: 24 mL, 30 bar of methane, 363 K. [e] $Pd(OAc)_2$: 10 μmol, quinone: 20 μmol, $NaNO_2$: 10 μmol, 1 atm of O_2, 54 atm of methane, 353 K. [f] $Co(OAc)_2{\cdot}2H_2O$: 3.8 mol%, HTFA/TFAA = 10 : 60, 20 bar of methane, 10 bar of O_2, 453 K. [g] Catalyst: 0.01 mmol, $[K_2S_2O_8]$ = 10 mmol, [TFAA] = 24 mmol, HTFA: 30 g, under 20 bars of methane, 353 K. [h] [CuO] = 9.4 mM, $[K_2S_2O_8]$ = 0.3 M, HTFA: 23 g, TFAA: 5 g, 5.2 bar of methane, 383 K. [i] Catalyst: 3 mol%, $[B_2pin_2]$ = 0.13 M, 3500 kPa of methane, 423 K. [j] Catalyst: 0.5 mol%, dmpe: 1.0 mol%, B_2pin_2: 20 mol%, 3447 kPa of methane, 423 K. [k] Catalyst: 0.035 mol%, B_2pin_2: 0.0512 mmol, 500 psi of methane, 423 K. [l] F_{27}–$Tp^{4Bo,3CF2CF3}Ag$: 0.03 mmol, $N_2CHCOOEt$: 3.0 mmol, 160 atm of methane, 313 K. [m] $[RhCl_3]$ = 0.01 M, [HCl] = 0.13 M, methane (800 psi), CO (200 psi), and O_2 (100 psi), 373 K. [n] $[PdSO_4]$ = 20 mM, 27.2 atm of methane, 453 K. [o] $[VO\{N(CH_2CH_2O)_3\}]$ = 0.04 μmol, $K_2S_2O_8$: 4.2 mmol, 12 atm of methane, 15 atm of CO, 353 K. [p] $Fe(TFA)_3$: 0.025 mmol, O_2: 15 mmol, under 100 psig of methane, 278 K, 370 nm LED. [q] $Ce(OTf)_3$: 0.01 mol%, CCl_3CH_2OH: 20 mol%, TBACl: 0.05 mol%, DBAD: 1 equivalent, 5000 kPa of methane, R.T. 400 nm LED. [r] TBADT: 0.5 mol%, [alkene] = 0.02 M, 45 bar of methane, R.T., 365 nm LED.

hydrophobic SCS close to the catalytically active metal centre (Schemes 19–21).

7. Fe–NHC complex having a hydrophobic cavity for "catch-and-release" oxidation of methane

Kojima and co-workers have synthesized Fe^{II} complexes bearing an *N*-heterocyclic carbene (NHC) ligand, $[Fe^{II}(^{H}PY_4Cl_2BIm)(OH_2)]^{2+}$, which have been reported to exhibit the reactivity in C–H oxidation using $Na_2S_2O_8$ as an ET oxidant in H_2O, showing high selectivity to afford 2-electron-oxidized products.[61] Based on this observation, as well as inspired by the arrangement of the hydrophobic cavity near the active iron centre in sMMOs, they have prepared Fe^{II} complexes bearing *N*-heterocyclic carbene ligands, $[Fe^{II}(^{R}PY_4Cl_2BIm)(NCMe)]^{2+}$ (R = mesityl (Mes), anthracenyl (Ant)).[62] Among those Fe^{II}–NHC complexes prepared, $[Fe^{II}(^{Ant}PY_4Cl_2BIm)(NCMe)]^{2+}$ has a hydrophobic SCS constructed from four anthracenyl moieties near a mononuclear iron centre (Fig. 6a).[62] The iron catalyst can trap one methane molecule into the hydrophobic SCS in aqueous media. The association constant of methane with $[Fe^{II}(^{Ant}PY_4Cl_2BIm)(OD_2)]^{2+}$ at 298 K has been determined to be $(2.1 \pm 0.4) \times 10^3$ M^{-1}, which is relatively high compared with the values reported so far for methane encapsulation.[62–67] The iron catalyst having a densely surrounded and rigid hydrophobic SCS has allowed us to observe a total TON of 5.0×10^2 with 83% methanol selectivity in a 3 h methane oxidation reaction using sodium persulfate as an oxidant (reaction conditions: [catalyst] = 1.0 mM, $[Na_2S_2O_8]$ = 5.0 mM, $P(CH_4)$ = 0.98 MPa, T = 323 K, $H_2O:CH_3CN$ = 95 : 5) (Fig. 6b). In this catalytic system, a hydrophobic CH_4 molecule is captured in the hydrophobic SCS of $[Fe^{II}(^{Ant}PY_4Cl_2BIm)(OH_2)]^{2+}$, which is formed by ligand substitution of CH_3CN in $[Fe^{II}(^{Ant}PY_4Cl_2BIm)(NCMe)]^{2+}$ with H_2O. $[Fe^{II}(^{Ant}PY_4Cl_2BIm)(OH_2)]^{2+}$ undergoes proton-coupled electron-transfer (PCET) oxidation to generate an Fe^{IV}–oxo complex ($[Fe^{IV}(O)(^{Ant}PY_4Cl_2BIm)]^{2+}$), which hydroxylates the CH_4 molecule (Fig. 6c). The hydroxylation affords a methanol-bound intermediate, Fe^{II}–$O(H)CH_3$, as a result of the oxygen-rebound mechanism. The putative Fe^{II}–$O(H)CH_3$ intermediate undergoes ligand substitution with H_2O to release the hydrophilic methanol molecule into the aqueous media to accomplish the catalytic cycle.[62] The high TON

Table 2 Summary of the catalytic activities of methane oxidation

Catalysts	Oxidants	Solvent	Reaction time	Total TON	Selectivities					Ref.
					MeOOH	MeOH	HCHO	HCOOH	CO_2	
cis-$[Ru(dmp)_2(OH_2)_2]^{2+a}$	H_2O_2	H_2O	30 h	125	—	75%	25%	—	Trace	36
$[Cu^ICu^ICu^I(7\text{–}N\text{–}Etppz)]^{+b}$	O_2	MeCN	1 h	18	—	100%	—	—	—	40
$[Cu_2(\mu\text{-}OH)(6\text{-}hpa)]^{3+c}$	H_2O_2	MeCN : H_2O = 4 : 1	3 h	50.4	—	85%	15%	—	—	42
$(FePc^tBu_4)_2N^d$	H_2O_2	H_2O	20 h	84	—	—	75%	25%	—	43
$[(TPP)Fe^{III}(\mu\text{-}N)Fe^{IV}(TPP)]^0\text{–}SiO_2{}^e$	*m*CPBA	H_2O	3 h	41	—	—	—	100%	—	47
$[(Por)Fe\text{–}N\text{–}Fe(Pc)]^{5+}\text{–}SiO_2{}^f$	H_2O_2	H_2O	8 h	30	—	32%	6%	62%	—	49
$[(Por)Fe\text{–}N\text{–}Fe(Pc)\text{–}Cu\text{–}TPPS]^+\text{–}SiO_2{}^f$	H_2O_2	H_2O	8 h	44	—	—	—	—	—	49
$[(Por)Fe\text{–}N\text{–}Fe(Pc)\text{–}Ni\text{–}TPPS]^+\text{–}SiO_2{}^f$	H_2O_2	H_2O	8 h	47	—	—	—	—	—	49
$(FePc(12\text{-}crown\text{-}4)_4)_2N\text{–}SiO_2{}^f$	H_2O_2	H_2O	8 h	26	—	22%	37%	42%	—	50
$(FePc^tMe_8)_2N\text{–}SiO_2{}^f$	H_2O_2	H_2O	16 h	147	—	7%	23%	71%	—	51
$[Cu^{II}(TREN)]^{2+}\text{–}SiO_2{}^g$	H_2O_2	H_2O	20 h	0.6	17%	—	—	83%	—	58
$[Cu^{II}(Hm\text{–}TREN)]^{2+}\text{–}SiO_2{}^g$	H_2O_2	H_2O	20 h	1.8	—	17%	6%	78%	—	58
$V(TKA)\text{–}SiO_2{}^g$	H_2O_2	H_2O	20 h	7.4	4%	4%	3%	89%	—	58
$V(Hm\text{–}TKA)\text{–}SiO_2{}^g$	H_2O_2	H_2O	20 h	6.6	—	15%	12%	73%	—	58
$V(Hm\text{–}BINOL\text{–}TKA)\text{–}SiO_2{}^g$	H_2O_2	H_2O	20 h	13.2	—	5%	18%	77%	—	58
$V(Bz\text{–}BINOL\text{–}TKA)\text{–}SiO_2{}^g$	H_2O_2	H_2O	20 h	18.3	—	4%	21%	75%	—	58
$[Fe^{II}(TPA)]^{2+}\text{–}SiO_2{}^g$	H_2O_2	H_2O	20 h	4.7	15%	—	49%	36%	—	58
$[Fe^{II}(Hm\text{–}TPA)]^{2+}\text{–}SiO_2{}^g$	H_2O_2	H_2O	20 h	9.2	15%	12%	22%	51%	—	58
$[Fe^{II}(^HPY_4Cl_2BIm)(NCMe)]^{2+h}$	$Na_2S_2O_8$	D_2O : CD_3CN = 95 : 5	3 h	64	—	38%	—	62%	—	62
$[Fe^{II}(^{Mes}PY_4Cl_2BIm)(NCMe)]^{2+h}$	$Na_2S_2O_8$	D_2O : CD_3CN = 95 : 5	3 h	101	—	71%	—	29%	—	62
$[Fe^{II}(^{Ant}PY_4Cl_2BIm)(NCMe)]^{2+h}$	$Na_2S_2O_8$	D_2O : CD_3CN = 95 : 5	3 h	500	—	83%	—	17%	—	62

[a] Reaction conditions: catalyst: 0.1 μmol, 30% aqueous H_2O_2: 0.1 mmol, under 4 atm of methane, 348 K. [b] [Catalyst] = 8 mM, [H_2O_2] = 160 mM, [CH_4] = 11 mM, under an O_2 atmosphere, 1 h, 278 K. [c] Catalyst: 0.03 μmol, H_2O_2: 300 μmol, Et_3N: 0.3 μmol, 8 MPa of methane, 323 K. [d] Catalyst: 0.925 μmol, H_2O_2: 678 μmol, 32 bar of methane, 323 K. [e] Catalyst: 1.1 μmol, *m*CPBA: 105 μmol, 32 bar of methane, 333 K. [f] [Catalyst] = 55 μM, [H_2O_2] = 189 mM, [TFA] = 51 mM, 1 MPa of methane, 333 K. [g] Catalyst: 1 μmol, [H_2O_2] = 0.33 M, 30 bar of methane, 333 K. [h] [Catalyst] = 1 μM, [$Na_2S_2O_8$] = 5 mM, 0.98 MPa of methane, 323 K.

and methanol selectivity in catalytic methane oxidation have been achieved by trapping a hydrophobic methane molecule in the hydrophobic SCS and by releasing a hydrophilic methanol molecule from the hydrophobic SCS into the surrounding aqueous medium. Kojima and co-workers have proved the validity of the "catch and release" strategy mimicking the catalytic performance of sMMOs for efficient and selective conversion of methane to methanol in aqueous medium (Fig. 7).

8. Summary and outlook

In this minireview, we have surveyed homogeneous catalysts for functionalization of methane. Tables 1 and 2 summarize the state-of-the-art functionalization of methane using homogeneous molecular catalysts.

While Hg and Pt catalysts show high efficiency and selectivity in the conversion of methane to MBS or MSA, the cost of product manipulation is high due to the need for water addition for hydrolysis of the products to obtain methanol. A Pd(II) catalyst can perform the formation of MeTFA using quinone as an electron mediator and O_2 as a terminal oxidant through the C–H activation in HTFA and reductive elimination of the product: this reaction system is reminiscent of the Wacker process to oxidize ethylene to produce acetaldehyde.[68] C–H activation of methane has been made by using late-transition-metal complexes such as Ru, Rh, and Ir complexes as catalysts to achieve borylation of methane through C–H activation as summarized in Table 1. An Ag(I) catalyst can perform the conversion of $N_2CHCOOEt$ to CH_3CH_2COOEt in sc-CO_2.

Photocatalytic methane oxidation has been achieved using Ce^{IV}–chloro complexes and a TFA salt of Fe^{III} as catalysts under photoirradiation. In the case of Ce^{IV} salts, photoirradiation causes charge transfer from negatively charged ligands to the Ce^{IV} centre to generate radical species, which is responsible for hydrogen abstraction from methane to form oxidized products. Furthermore, photo-excited $*[W_{10}O_{32}]^{4-}$ enables hydrogen atom transfer from methane to form $CH_3^{\bullet}$, reacting with alkenes to afford hydroalkylated products. Photocatalytic methane functionalization will be developed through various approaches including emerging molecular catalysts.[69]

Dinuclear and trinuclear copper complexes as well as μ-nitride iron phthalocyanine catalysts, inspired by the active sites of pMMOs and sMMOs, respectively, can catalyse methane oxidation using peroxides as oxidants under ambient conditions. The tricopper cluster catalyst shows a moderate TON with high methanol selectivity. On the other hand, μ-nitride iron phthalocyanine catalysts exhibit a high TON but low methanol selectivity in water due to decomposition or overoxidation by $^{\bullet}OH$ derived from the oxidants used. Furthermore, vanadium and iron catalysts with hydrophobic cavities constructed from hemicryptophane or BINOL moieties can improve the TON and methanol selectivity in water. Very recently, Kojima and co-workers have launched a "catch-and-release" strategy in aqueous medium, inspired by the functionality of the hydrophobic cavity near

the diiron active site of sMMOs. They have developed a catalyst with a hydrophobic SCS constructed from four anthracenyl moieties attached to the NHC ligand. The catalyst can convert methane into methanol with a total TON of 500 for 3 h and 83% methanol selectivity. The "catch-and-release" strategy allows a hydrophobic methane molecule to be trapped in the hydrophobic SCS for oxidation, and the resulting hydrophilic methanol molecule is released into the surrounding aqueous solution.

Note that, in the arguments on methane oxidation using metal complexes having organic ligands, precaution should be taken to confirm that the origin of the carbon source of product(s) is exclusively methane by employing isotope-labelled methane, such as $^{13}CH_4$ (ref. 13, 15, 21, 26, 29–32 and 42) or CD_4.[39,46,62]

Toward the construction of a sustainable society, manipulation of methane is getting more important than ever in light of sustainable development goals (SDGs) to solve energy and environmental issues. By virtue of molecular catalysts, where we can fine-tune reactivity of metal centres by manipulating ligand sets, electronic properties and structures of SCSs, we can pave the way for effective and selective utilization of methane as a C1 resource under milder and sustainable conditions, as enzymes do so. The stability of molecular catalysts would be of concern; however, a certain range of robustness can be gained by introduction of suitable substituents at appropriate positions of a ligand. Molecular catalysts for methane functionalization should be developed in many ways in terms of not only technical improvement for the catalysis but also accumulation of fundamental scientific knowledge in our toolbox, which should be applicable to many kinds of reactions we need.

Conflicts of interest

There are no conflicts to declare.

Acknowledgements

This work has been supported by CREST (JPMJCR16P1) from Japan Science and Technology Agency (JST).

Notes and references

1 (*a*) H. Arakawa, *et al.*, *Chem. Rev.*, 2001, **101**, 953; (*b*) R. Horn and R. Schlögl, *Catal. Lett.*, 2015, **145**, 23.

2 X. Zhen and Y. Wang, *Renewable Sustainable Energy Rev.*, 2015, **52**, 477.

3 *World Energy Outlook*, International Energy Agency, 2022.

4 (*a*) P. Schwach, X. Pa and X. Bao, *Chem. Rev.*, 2017, **117**, 8497; (*b*) *AR6 WGI Report – List of corrigenda to be implemented*, IPCC, 2021; (*c*) see also ref. 3.

5 (*a*) J. R. Rostrup-Nielsen, J. S. Sehested and J. K. Nørskov, *Adv. Catal.*, 2002, **47**, 65; (*b*) M. Ravi, M. Ranocchiari and J. A. van Bokhoven, *Angew. Chem., Int. Ed.*, 2017, **56**, 16464.

6 Some representative references: TiO_2-supported metal species: (*a*) J. Xie, R. Jin, Y. Bi, Q. Ruan, Y. Deng, Y. Zhang, S. Yao, G. Sankar, D. Ma and J. Tang, *Nat. Catal.*, 2018, **1**, 889; (*b*) H. Song, X. Meng, S. Wang, W. Zhou, S. Song, T. Kako and J. Ye, *ACS Catal.*, 2020, **10**, 14318; Au-Pd colloids: (*c*) M. H. Ab Rahim, M. M. Forde, R. L. Jenkins, C. Hammond, Q. He, N. Dimitratos, J. A. Lopez-Sanchez, A. F. Carley, S. H. Taylor, D. J. Willock, D. M. Murphy, C. J. Kiely and G. J. Hutchings, *Angew. Chem., Int. Ed.*, 2012, **52**, 1280; (*d*) N. Agarwal, S. J. Freakley, R. U. McVicker, S. M. Althahban, N. Dimitratos, Q. He, D. J. Morgan, R. L. Jenkins, D. J. Willock, S. H. Taylor, C. J. Kiely and G. J. Hutchings, *Science*, 2017, **358**, 223; (*e*) R. Serra-Maia, F. M. Michel, T. A. Douglas, Y. Kang and E. A. Stach, *ACS Catal.*, 2021, **11**, 2837; Metal oxide: (*f*) S. Park, J. M. Vohs and R. J. Gorte, *Nature*, 2000, **406**, 265; (*g*) C. Okolie, Y. F. Belhseine, Y. Lyu, M. M. Yung, M. H. Engelhard, L. Kovarik, E. Stavitski and C. Sievers, *Angew. Chem., Int. Ed.*, 2017, **56**, 13876; (*h*) H. Song, X. Meng, S. Wang, W. Zhou, X. Wang, T. Kako and J. Ye, *J. Am. Chem. Soc.*, 2019, **141**, 20507; MOF: (*i*) M. C. Simons, S. D. Prinslow, M. Babucci, A. S. Hoffman, J. Hong, J. G. Vitillo, S. R. Bare, B. C. Gates, C. C. Lu, L. Gagliardi and A. Bhan, *J. Am. Chem. Soc.*, 2021, **143**, 12165; (*j*) N. Antil, M. Chauhan, N. Akhtar, R. Kalita and K. Manna, *J. Am. Chem. Soc.*, 2023, **145**, 6156; (*k*) B. An, Z. Li, Z. Wang, X. Zeng, X. Han, Y. Cheng, A. M. Sheveleva, Z. Zhang, F. Tuna, E. J. L. McInnes, M. D. Frogley, A. J. Ramirez-Cuesta, L. S. Natrajan, C. Wang, W. Lin, S. Yang and M. Schröder, *Nat. Mater.*, 2022, **21**, 932; P_4O_{10}: (*l*) N. Dietl, M. Engeser and H. Schwarz, *Angew. Chem., Int. Ed.*, 2009, **48**, 4861; Pd/C: (*m*) M. Lin and A. Sen, *J. Am. Chem. Soc.*, 1992, **114**, 7308; (*n*) M. Lin, T. Hogan and A. Sen, *J. Am. Chem. Soc.*, 1997, **119**, 6048Zeolite: (*o*) C. Hammond, M. M. Forde, M. H. Ab Rahim, A. Thetford, Q. He, R. L. Jenkins, N. Dimitratos, J. A. Lopez-Sanchez, N. F. Dummer, D. M. Murphy, A. F. Carley, S. H. Taylor, D. J. Willock, E. E. Stangland, J. Kang, H. Hagen, C. J. Kiely and G. J. Hutchings, *Angew. Chem., Int. Ed.*, 2012, **51**, 5129; (*p*) C. Hammond, R. L. Jenkins, N. Dimitratos, J. A. Lopez-Sanchez, M. H. Ab Rahim, M. M. Forde, A. Thetford, D. M. Murphy, H. Hagen, E. E. Stangland, J. M. Moulijn, S. H. Taylor, D. J. Willock and G. J. Hutchings, *Chem. – Eur. J.*, 2012, **18**, 15735; (*q*) W. Huang, S. Zhang, Y. Tang, Y. Li, L. Nguyen, Y. Li, J. Shan, D. Xiao, R. Gagne, A. I. Frenkel and F. F. Tao, *Angew. Chem., Int. Ed.*, 2016, **55**, 13441; (*r*) B. Ipek and R. F. Lobo, *Chem. Commun.*, 2016, **52**, 13401; (*s*) J. Shan, M. Li, L. F. Allard, S. Lee and M. Flytzani-Stephanopoulos, *Nature*, 2017, **551**, 605; (*t*) V. L. Sushkevich, D. Palagin, M. Ranocchiari and J. A. van Bokhoven, *Science*, 2017, **356**, 523; (*u*) E. Tabor, M. Lemishka, Z. Sobalik, K. Mlekodaj, P. C. Andrikopoulos, J. Dedecek and S. Sklenak, *Commun. Chem.*, 2019, **2**, 71; (*v*) L. Sun, Y. Wang, C. Wang, Z. Xie, N. Guan and L. Li, *Chem*, 2021, **7**, 1557.

7 (*a*) Y.-R. Luo, *Handbook of bond dissociation energies in organic compounds*, CRC Press LLC, Boca Raton, FL, 1st edn, 2003; (*b*) S. J. Blanksby and G. B. Ellison, *Acc. Chem. Res.*, 2003, **36**, 255.

8 For pMMO: (*a*) M. A. Culpepper and A. C. Rosenzweig, *Crit. Rev. Biochem. Mol. Biol.*, 2012, **47**, 483; (*b*) C. W. Koo and

A. C. Rosenzweig, *Chem. Soc. Rev.*, 2021, **50**, 3424; (*c*) R. L. Lieberman and A. C. Rosenzweig, *Nature*, 2005, **434**, 171; (*d*) V. C.-C. Wang, S. Maji, P. P.-Y. Chen, H. K. Lee, S. S.-F. Yu and S. I. Chan, *Chem. Rev.*, 2017, **117**, 8754; (*e*) W. Peng, X. Qu, S. Shaik and B. Wang, *Nat. Catal.*, 2021, **4**, 266.

9 For sMMO: (*a*) V. Srinivas, *et al.*, *J. Am. Chem. Soc.*, 2020, **142**, 14249; (*b*) A. C. Rosenzweig, C. A. Frederick, S. J. Lippard and P. Nordlund, *Nature*, 1993, **366**, 537; (*c*) M.-H. Baik, M. Newcomb, R. A. Friesner and S. J. Lippard, *Chem. Rev.*, 2003, **103**, 2385.

10 (*a*) R. Banerjee and J. D. Lipscomb, *Acc. Chem. Res.*, 2021, **54**, 2185; (*b*) R. G. Castillo, R. Banerjee, C. J. Allpress, G. T. Rohde, E. Bill, L. Que Jr., J. D. Lipscomb and S. DeBeer, *J. Am. Chem. Soc.*, 2017, **139**, 18024; (*c*) S.-K. Lee, B. G. Fox, W. A. Froland, J. D. Lipscomb and E. Münck, *J. Am. Chem. Soc.*, 1993, **115**, 6450.

11 (*a*) L. Que Jr. and W. B. Tolman, *Nature*, 2008, **455**, 333; (*b*) A. R. McDonald and L. Que Jr., *Coord. Chem. Rev.*, 2013, **257**, 414; (*c*) M. Guo, Y.-M. Lee, S. Fukuzumi and W. Nam, *Coord. Chem. Rev.*, 2021, **435**, 213807; (*d*) W. Nam, Y.-M. Lee and S. Fukuzumi, *Acc. Chem. Res.*, 2018, **51**, 2014; (*e*) W. Zhu, A. Kumar, J. Xiong, M. J. Abernathy, X.-X. Li, M. S. Seo, Y.-M. Lee, R. Sarangi, Y. Guo and W. Nam, *J. Am. Chem. Soc.*, 2023, **145**, 4389; (*f*) V. A. Larson, B. Battistella, K. Ray, N. Lehnert and W. Nam, *Nat. Rev. Chem.*, 2020, **4**, 404; (*g*) G. L. Tripodi, M. M. J. Dekker, J. Roithová and L. Que Jr., *Angew. Chem.*, 2021, **60**, 7126.

12 J. C. Snyder and A. V. Grosse, *US Pat.*, 2493038, 1950.

13 R. A. Periana, D. J. Taube, E. R. Evitt, D. J. Löffler, P. R. Wentrcek, G. Voss and T. Masuda, *Science*, 1993, **259**, 340.

14 (*a*) A. E. Shilov, *Activation of saturated hydrocarbons by transition metal complexes*, D. Reidel Publishing Co.: Dordrecht, The Netherlands, 1984; (*b*) J. A. Labinger and J. E. Bercaw, *Nature*, 2002, **417**, 507; (*c*) A. E. Shilov and G. B. Shul'pin, *Russ. Chem. Rev.*, 1987, **56**, 442; (*d*) G. A. Luinstra, L. Wang, S. S. Stahl, L. A. Labinger and J. E. Bercaw, *J. Org. Chem.*, 1995, **504**, 75.

15 R. A. Periana, D. J. Taube, S. Gamble, H. Taube, T. Satoh and H. Fujii, *Science*, 1998, **280**, 560.

16 O. A. Mironov, S. M. Bischof, M. M. Konnick, B. G. Hashiguchi, V. R. Ziatdinov, W. A. Goddard III, M. Ahlquist and R. A. Periana, *J. Am. Chem. Soc.*, 2013, **135**, 14644.

17 (*a*) T. Zimmermann, M. Soorholtz, M. Bilke and F. Schüth, *J. Am. Chem. Soc.*, 2016, **138**, 12395; (*b*) T. Zimmermann, M. Bilke, M. Soorholtz and F. Schüth, *ACS Catal.*, 2018, **8**, 9262.

18 H. T. Dang, H. W. Lee, J. Lee, H. Choo, S. H. Hong, M. Cheong and H. Lee, *ACS Catal.*, 2018, **8**, 11854.

19 C. Díaz-Urrutia and T. Otto, *Science*, 2019, **363**, 1326.

20 (*a*) M. Muehlhofer, T. Strassner and W. A. Herrmann, *Angew. Chem., Int. Ed.*, 2002, **41**, 1745; (*b*) S. Ahrens, A. Zeller, M. Taige and T. Strassner, *Organometallics*, 2006, **25**, 5409; (*c*) D. Meyer, M. A. Taige, A. Zeller, K. Hohlfeld, S. Ahrens and T. Strassner, *Organometallics*, 2009, **28**, 2142.

21 Z. An, X. Pan, X. Liu, X. Han and X. Bao, *J. Am. Chem. Soc.*, 2006, **128**, 16028.

22 T. Strassner, S. Ahrens, M. Muehlhofer, D. Munz and A. Zeller, *Eur. J. Inorg. Chem.*, 2013, 3659.

23 S.-H. Cheong, D. Kim, H. T. Dang, D. Kim, B. Seo, M. Cheong, S. H. Hong and H. Lee, *J. Catal.*, 2022, **413**, 803.

24 M. Ravi and J. A. van Bokhoven, *ChemCatChem*, 2018, **10**, 2383.

25 A. K. Cook, S. D. Schimler, A. J. Matzger and M. S. Sanford, *Science*, 2016, **351**, 1421.

26 K. T. Smith, S. Berritt, M. González-Moreiras, S. Ahn, M. R. Smith III, M.-H. Baik and D. J. Mindiola, *Science*, 2016, **351**, 1424.

27 O. Staples, M. S. Ferrandon, G. P. Laurent, U. Kanbur, A. J. Kropf, M. R. Gau, P. J. Carroll, K. McCullough, D. Sorsche, F. A. Perras, M. Delferro, D. M. Kaphan and D. J. Mindiola, *J. Am. Chem. Soc.*, 2023, **145**, 7992.

28 A. Caballero, E. Despagnet-Ayoub, M. M. Díaz-Requejo, A. Díaz-Rodríguez, M. E. González-Núñez, R. Mello, B. K. Muñoz, W.-S. Ojo, G. Asensio, M. Etienne and P. J. Pérez, *Science*, 2011, **332**, 835.

29 M. Lin and A. Sen, *Nature*, 1994, **368**, 613.

30 R. A. Periana, O. Mironov, D. Taube, G. Bhalla and C. Jones, *Science*, 2003, **301**, 814.

31 M. V. Kirillova, M. L. Kuznetsov, P. M. Reis, J. A. L. da Silva, J. J. R. Fraústo da Silva and A. J. L. Pombeiro, *J. Am. Chem. Soc.*, 2007, **129**, 10531.

32 N. Coutard, J. M. Goldberg, H. U. Valle, Y. Cao, X. Jia, P. D. Jeffrey, T. B. Gunnoe and J. T. Groves, *Inorg. Chem.*, 2021, **61**, 759.

33 A. Hu, J.-J. Guo, H. Pan and Z. Zuo, *Science*, 2018, **361**, 668.

34 Q. Yang, Y.-H. Wang, Y. Qiao, M. Gau, P. J. Carroll, P. J. Walsh and E. J. Schelter, *Science*, 2021, **372**, 847.

35 G. Laudadio, Y. Deng, K. van der Wal, D. Ravelli, M. Nuño, M. Fagnoni, D. Guthrie, Y. Sun and T. Noël, *Science*, 2020, **369**, 92.

36 (*a*) A. S. Goldstein and R. S. Drago, *J. Chem. Soc., Chem. Commun.*, 1991, 21; (*b*) A. S. Goldstein, R. H. Beer and R. S. Drago, *J. Am. Chem. Soc.*, 1994, **116**, 2424.

37 P. P.-Y. Chen, R. B.-G. Yang, J. C.-M. Lee and S. I. Chan, *Proc. Natl. Acad. Sci. U. S. A.*, 2007, **104**, 14571.

38 S. I. Chan, Y.-J. Lu, P. Naganobu, S. Maji, M.-C. Hung, M. M. Lee, I.-J. Hsu, P. D. Minh, J. C.-H. Lai, K. Y. Ng, S. Ramalingam, S. S.-F. Yu and M. K. Chan, *Angew. Chem., Int. Ed.*, 2013, **52**, 3731.

39 P. P.-Y. Chen, P. Naganobu, S. S.-F. Yu and S. I. Chan, *ChemCatChem*, 2014, **6**, 429.

40 P. Naganobu, S. S.-F. Yu, R. Ramu and S. I. Chan, *Catal. Sci. Technol.*, 2014, **4**, 930.

41 Y.-H. Chen, C.-Q. Wu, P.-H. Sung, S. I. Chan and P. P.-Y. Chen, *ChemCatChem*, 2020, **12**, 3088.

42 H. Takahashi, K. Wada, K. Tanaka, K. Fujikawa, Y. Hitomi, T. Endo and M. Kodera, *Bull. Chem. Soc. Jpn.*, 2022, **95**, 1148.

43 L. A. Bottomley, J.-N. Gorce, V. L. Goedken and C. Ercolani, *Inorg. Chem.*, 1985, **24**, 3733.

44 A. B. Solokin, E. V. Kudrik and D. Bouchu, *Chem. Commun.*, 2008, 2562.

45 P. Afanasiev, E. V. Kudrik, J.-M. M. Millet, D. Bouchu and A. B. Solokin, *Dalton Trans.*, 2011, **40**, 701.
46 M. G. Quesne, D. Senthilnathan, D. Singh, D. Kumar, P. Maldivi, A. B. Solokin and S. P. de Visser, *ACS Catal.*, 2016, **6**, 2230.
47 E. V. Kudrik, P. Afanasiev, L. X. Alvarez, P. Dubourdeaux, M. Clémancey, J.-M. Latour, G. Blondin, D. Bouchu, F. Albrieux, S. E. Nefedov and A. B. Sorokin, *Nat. Chem.*, 2012, **4**, 1024.
48 N. Mihara, Y. Yamada, H. Takuya, Y. Kitagawa, K. Igawa, K. Tomooka, H. Fujii and K. Tanaka, *Chem. – Eur. J.*, 2019, **25**, 3369.
49 Y. Yamada, K. Morita, N. Mihara, K. Igawa, K. Tomooka and K. Tanaka, *New J. Chem.*, 2019, **43**, 11477.
50 Y. Yamada, J. Kura, Y. Toyoda and K. Tanaka, *New J. Chem.*, 2020, **44**, 19179.
51 Y. Yamada, J. Kura, Y. Toyoda and K. Tanaka, *Dalton Trans.*, 2021, **50**, 6718.
52 Ü. İşci, A. S. Faponle, P. Afanasiev, F. Albrieux, V. Briois, V. Ahsen, F. Dumoulin, A. B. Sorokin and S. P. de Visser, *Chem. Sci.*, 2015, **6**, 5063.
53 G. V. Nizova, G. Süss-Fink and G. B. Shul'pin, *Chem. Commun.*, 1997, 397.
54 G. B. Shul'pin, G. V. Nizova, Y. N. Kozlov, L. G. Cuervo and G. Süss-Fink, *Adv. Synth. Catal.*, 2004, **346**, 317.
55 Q. Yuan, W. Deng, Q. Zhang and Y. Wang, *Adv. Synth. Catal.*, 2007, **349**, 1199.
56 Y. Naruta, F. Tani, N. Ishibara and K. Maruyama, *J. Am. Chem. Soc.*, 1991, **113**, 6865.
57 J. T. Groves and P. Viski, *J. Org. Chem.*, 1990, **55**, 3628.
58 S. A. Ikbal, C. Colomban, D. Zhang, M. Delecluse, T. Brotin, V. Dufaud, J.-P. Dutasta, A. B. Sorokin and A. Martinez, *Inorg. Chem.*, 2019, **58**, 7220.
59 D. Zhang, K. Jamieson, L. Guy, G. Gao, J.-P. Dutasta and A. Martinez, *Chem. Sci.*, 2017, **8**, 789.
60 D. Zhang, J.-P. Dutasta, V. Dufaud, L. Guy and A. Martinez, *ACS Catal.*, 2017, **7**, 7340.
61 (*a*) H. Fujisaki, T. Ishizuka, Y. Shimoyama, H. Kotani, Y. Shiota, K. Yoshizawa and T. Kojima, *Chem. Commun.*, 2020, **56**, 9783; (*b*) H. Fujisaki, M. Okamura, S. Hikichi and T. Kojima, *Chem. Commun.*, 2023, **59**, 3265.
62 H. Fujisaki, T. Ishizuka, H. Kotani, Y. Shiota, K. Yoshizawa and T. Kojima, *Nature*, 2023, **616**, 476.
63 N. Branda, R. Wyler and J. Rebek Jr., *Science*, 1994, **263**, 1267.
64 L. Garel, J. P. Dutasta and A. Collet, *Angew. Chem., Int. Ed. Engl.*, 1993, **32**, 1169.
65 J. Nakazawa, J. Hagiwara, M. Mizuki, Y. Shimazaki, F. Tani and Y. Naruta, *Angew. Chem., Int. Ed.*, 2005, **44**, 3744.
66 A. V. Leontiev, A. W. Saleh and D. M. Rudkevich, *Org. Lett.*, 2007, **9**, 1753.
67 Y. Ruan, P. W. Peterson, C. M. Hadad and J. D. Badjić, *Chem. Commun.*, 2014, **50**, 9086.
68 R. A. Fernandes, A. K. Jha and P. Kumar, *Catal. Sci. Technol.*, 2020, **10**, 7448.
69 Y. Jiang, Y. Fan, S. Li and Z. Tang, *CCS Chem.*, 2023, **5**, 30.

